Diamond Nanostructures and Nanoparticles: Electrochemical Properties and Applications

Nianjun Yang and Xin Jiang

Abstract Macro-sized diamond films have been widely applied as the electrode for electrochemical and electroanalytical applications. Due to the non-uniform doping in diamond, boundary effects, and the varied ratios of graphite to diamond, only averaged electrochemical signals are detected over the full electrode. The studies of diamond electrochemistry at the nanoscale are thus highly required. In this chapter we overview recent progress and achievements about electrochemical properties and applications of diamond nanostructures and nanoparticles. After a brief introduction of the formation of these nanostructures and nanoparticles, electrochemical behavior of diamond nanostructures (e.g., diamond nanotexures, nanowires, networks, etc.) and nanoparticles (undoped, doped nanoparticles) in the presence/absence of redox probes is summarized. Their electroanalytical (e.g., electrochemical, biochemical sensing, etc.) and electrochemical (e.g., energy storage using capacitors and batteries, electrocatalysis, etc.) applications are shown. Diamond nanoelectrode array is introduced and highlighted as a promising tool to investigate diamond electrochemistry at the nanoscale as well.

Keywords Electrochemistry · Electroanalysis · Diamond · Nanowires · Nanoparticles · Nanoelectrodes and arrays

1 Introduction

Iwaki et al. in 1983 [1] and later Pleskov et al. in 1987 [2] introduced diamond as an electrode material. Since then boron-doped diamond has been recognized as one of the best electrode materials. It shows numerous unique physical and chemical

N. Yang (✉) · X. Jiang (✉)
Institute of Materials Engineering, University of Siegen,
57076 Siegen, Germany
e-mail: nianjun.yang@uni-siegen.de

X. Jiang
e-mail: xin.jiang@uni-siegen.de

N. Yang et al. (eds.), *Carbon Nanoparticles and Nanostructures*,
Carbon Nanostructures, DOI 10.1007/978-3-319-28782-9_9

properties [3–5], such as (i) high chemical stability in harsh environments and/or at high voltage/current densities; (ii) weak or no surface bio-fouling; (iii) biocompatibility; (iv) low and stable capacitive currents in aqueous and non-aqueous solutions; and (v) a wide electrochemical potential window. Moreover, the diamond surface can be terminated with hydrogen, hydroxyl, and oxygen, which allow tuning the electronic properties of the solid/electrolyte interface with respect to energy alignments of interacting levels. Furthermore, diamond is ultra-hard (50–150 GaP) and various diamond nanostructures can be formed [6–9].

Many successful reports have been thus shown about the use of planar macroscopic diamond electrodes for electrochemistry, bio electrochemistry, electroanalysis, electrocatalysis, and environmental related applications [3–6]. However due to the non-uniform doping in diamond, boundary effects, and the varied ratios of graphite to diamond, in most studies only averaged electrochemical signals are detected over the full electrode. To solve this problem, the investigation of diamond electrochemistry at the nanoscale, in other words, electrochemistry of diamond nanostructures and nanoparticles, is highly needed. In this way the difference of electric and electrochemical properties from their bulk electrodes might be detected. The effect of the size, shape, and composition of diamond nanostructures and nanoparticles on their electrochemical properties can be clarified [10–12]. These studies will play significant role in their applications for electrochemical energy storage and conversion, electrocatalysis, electrochemical sensor development, and related fields.

We therefore summarize in this chapter recent progress and achievements about diamond electrochemistry using diamond nanostructures (e.g., nanotextures, nanowires) [13–56], diamond nanoparticles (un-doped and doped nanoparticles) [57–128], and diamond nanoelectrode arrays [129–132]. The applications of these nanostructures and nanoparticles for electroanalytical (e.g., electrochemical, biochemical sensing) and electrochemical applications (e.g., energy storage with capacitors and batteries, electrocatalysis, etc.) [133–141] are shown. Diamond nanoelectrode array is introduced and highlighted as a promising tool to investigate diamond electrochemistry at the nanoscale. After comparing the results published in literature, we close this chapter with a conclusion about the future and tendency of electrochemistry using diamond nanostructures and nanoparticles.

2 Diamond Nanostructures

2.1 Fabrication Approaches

Diamond nanostructures, including nanotextures (also called nanograss, nanowinkles, nanocone, etc.) with dimensions of typically a few nanometers, nanowires (also called nanoneedles, nanoforests, etc.) with lengths of a few micrometers, and networks (also called porous films, etc.) with pore sizes from few nanometers to

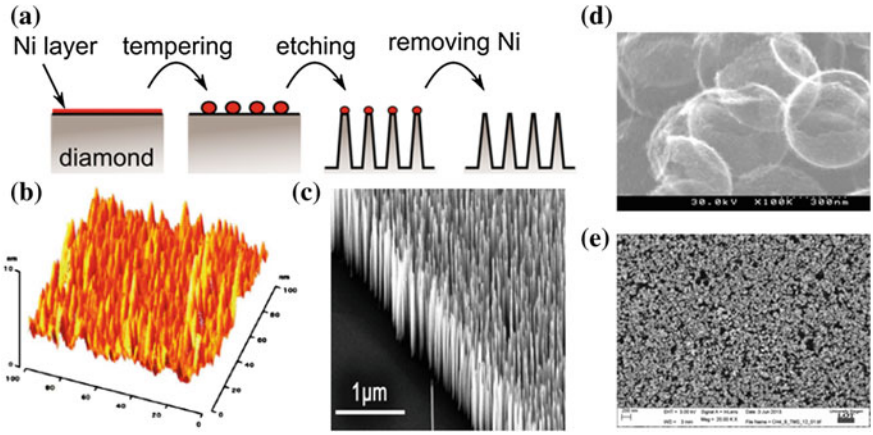

Fig. 1 **a** Schematic illustration of forming diamond nanowires using a top-down approach and Ni nanoparticles as the etching mask; **b** AFM tapping-mode image of diamond nanotextures; SEM images of **c** diamond nanowires, **d** diamond foam and **e** diamond networks [137]

micrometers have been fabricated using top-down, bottom-up, or template-free approaches. In the top-down approach, diamond is etched away with reactive ions in a plasma using an etching (hard) mask. Figure 1a shows schematically such an approach where nickel nanoparticles are applied as the etching mask. The morphology (e.g., size, length, density, etc.) of the resulting nanostructures are determined mainly by the etching mask (e.g., nature, size, shape, etc.) and etching conditions (e.g., temperature, gas, pressure, time, etc.). Various mask materials have been thus applied, including Al, SiO_2, Au, Ni, Mo, polymers, oxides, nitrides, and diamond nanoparticles, etc. [6–9]. For example, the etching mask of 5–10 nm diamond nanoparticles was applied to form diamond nanotextures [13]. With an etching time of 10 s the textures (1–5 nm in diameters, 11 nm in distance) were produced. One typical AFM tapping-mode image of such nanotextures is shown in Fig. 1b. If nickel nanoparticles were applied as the etching mask, the formed diamond nanowires [14] have a height of 1200 (±200) nm, a width of 35 (±5) nm, and a density of $\sim 10^{10}$ cm^{-2}, as shown in the SEM image in Fig. 1c. In a bottom-up approach, diamond nanostructures are produced by the overgrowth of other nanostructures. Up to the morphology of the templates, various diamond nanostructures have been formed [6–9]. The templates from silicon nanowires, carbon nanotubes (CNTs), SiO_2 spheres, etc. have been employed. Figure 1d shows one SEM image of diamond foam fabricated with the overgrowth of SiO_2 sphere. Figure 1e gives the SEM image of a diamond network [48], synthesized with a template-free approach, namely through selective and wet-chemical removal of silicon carbide from a diamond/SiC composite film with a mixture of HF and HNO_3.

2.2 Electrochemical Properties

Voltammetry and impedance were applied to characterize the interfacial properties (e.g., the real electrode areas, their electrochemical activities) of diamond nanotextures and nanowires [13–15]. The analysis of Mott-Schottky plots [13] in the absence of redox probes, the analysis of electrochemical impedance spectra using an electric equivalent circuit [15] and the cyclic voltammograms in the presence of redox probes were conducted to determine the surface areas of diamond nanostructures as well as the electrode processes of redox probes on diamond nanostructures based electrodes [13–15].

For example, Fig. 2 shows the Mott-Schottky plots of a smooth diamond electrode and diamond nanotextures based electrode (for an etching time of 10 s and using diamond nanoparticles as the etching mask) in 0.1 M pH 7.4 phosphate buffer. The measurements were done at a fixed frequency of 1.0 kHz. The built-in potential of diamond nanotextures, calculated by use of Mott-Schottky equation, was 1.6 V. Its surface area was 2.1 times higher than that of a smooth diamond [13].

Figure 3a shows the cyclic voltammograms of a smooth diamond electrode and diamond nanowires based electrode (using a top-down approach and nickel nanoparticles as the etching mask) in 0.1 M KCl. The surface area of diamond nanowires based electrode, calculated from the capacitive current, is 10-times larger than that of a smooth diamond electrode [14]. On such an electrode the electrode process of $Fe(CN)_6^{3-/4-}$ was quasi-reversible and diffusion-controlled, as shown in Fig. 3b. The calculated electrode active area of diamond nanowires based electrode is however only 1.5 times larger than that of a smooth diamond. Similar result, namely the electrode area calculated from the capacitive current is much larger than that from the Faradaic current of redox probes, was obtained on diamond networks [48]. This is because the faradaic current of ferri-/ferro- cyanide is dominated by their diffusion lengths of analytes, which are typically in the range

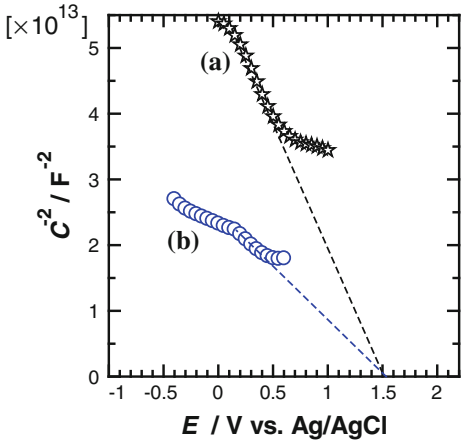

Fig. 2 Mott-Schottky plots of **a** a smooth diamond and (**b**) diamond nanotextures for an etching time of 10 s in 0.1 M pH 7.4 phosphate buffer at a fixed frequency of 1.0 kHz [13]

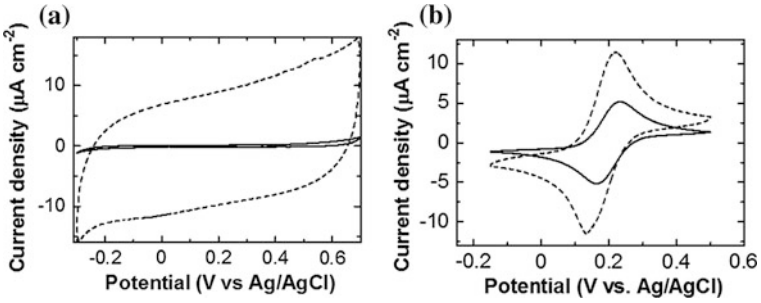

Fig. 3 Cyclic voltammograms of (solid lines) a smooth diamond electrode and (dashed lines) diamond nanowires based electrode in **a** 0.1 M KCl at a scan rate of 0.050 V s^{-1} and in **b** 1.0 mM $Fe(CN)_6^{3-/4-}$ + 0.1 M KCl at a scan rate of 0.1 V s^{-1} [14]

of tens of micrometers. Since the distance in between nanowires or diamond pores is much smaller than the value of diffusion lengths of analytes, diamond nanowires or diamond networks based electrode actually behaves as a macro-sized electrode [14].

2.3 Electrochemical Applications

Due to improved reactive sites, promoted electrocatalytic activities, and accelerated electron transfer rates, diamond nanotextures/nanowires are promising electrodes to improve the efficiency, sensitivity, selectivity and reproducibility of biomedical and chemical sensors [16–39]. Due to their wide electrochemical potential windows, enhanced surface areas, as well as high chemical stability, diamond nanostructures have been used for energy storage and related applications [42–56].

2.3.1 Electroanalytical Applications

Diamond nanostructures have been widely applied for electroanalytical applications [16–55], such as for electrochemical sensing of dopamine in the presence of ascorbic acid and uric acid [16, 17], for non-enzymatic monitoring of glucose [18–20], for the detection and immobilization of biomolecules (e.g., tryptophan [21, 22], tyrosine [22], catechol [23], and cytochrome c [24–26]), for enhanced electron transfer of shewanella loihica PV-4 [27], and for the construction of toxicity sensor by use of shewanella loihica PV-4 planktonic cells as the recognition element in bioelectrochemical systems [28].

For example, N-doped diamond nanowires showed excellent electrocatalytic activity towards the oxidation of ascorbic acid, dopamine, and uric acid. The electrocatalytic activity results from the increased sp^2 graphitic phase and the nanowire-like structure [17]. Diamond nanowires allowed non-enzymatic oxidation

of glucose [18–20]. On diamond nanowires (e.g., with the length of about 3 μm and the diameter from 10 to 50 nm), a detection limit of 60 μM glucose was reported [19]. A fast and stable glucose oxidation process (less than 20 s) was reported on diamond nanowires as well [18]. At 0.7 V (vs. SCE), the stable steady-state (only 8 % reduction after 150 repetitive cycles) oxidation current was linearly enhanced with the concentration of glucose from 0 to 7 mM. The sensitivity of these detections was 8.1 μA mM^{-1} cm^{-2} and the detection limit was 0.2 ± 0.01 μM [18]. On diamond nanowires (e.g., with 20 nm in diameter, 200 nm in length and 50 nm in distance), electrocatalytic detection of catechol was realized in a working concentration range of 5 to 100 μM with a sensitivity of 719.71 μA M^{-1} cm^{-2} and a detection limit of 1.3 μM [23]. Differential pulse voltammetric detection of tryptophan on diamond nanowires was reported with a detection limit of 5×10^{-7} M [21]. Simultaneous detection of tryptophan and tyrosine was conducted successfully as well by differential pulse voltammetry on diamond nanowires when the amount ratio of tryptophan to tyrosine was less than 0.5 [22].

Direct electrochemistry of cytochrome c was realized on the OH-terminated diamond nanotextrues [24–26]. As shown in Fig. 4a, diamond nanotextures act as molecular traps, leading to a more efficient electron transfer process. The surface coverage of cytochrome c on diamond nanotextures was evaluated to be 4.2×10^{12} cm^{-2} and its electron transfer rate constant was (1.43 ± 0.05) s^{-1}, higher than some of reported values [24–26]. The enhancement of electron transfer rate results from the electrostatic and hydrophobic interaction of cytochrome c with the OH-terminated diamond. Electrocatalytic reactions towards oxygen reduction as well as AFM tapping and scratching experiments in buffer [29–31] further confirmed that the electrostatic interaction controls coarse orientation of cytochrome c while hydrophobic interaction assists in the formation of the electron transfer complex, as schematically shown in Fig. 4b. Diamond nanograss showed an enhanced electron transfer from outer membrane c-type cytochromes of shewanella loihica PV-4 to the electrode [27]. Using such a shewanella loihica PV-4 planktonic cell as the recognition element in bioelectrochemical systems (BES), a toxicity sensor based on the electrochemical and impedance detection of tobramycin was proposed [28].

Decorated diamond nanotextures/nanowires with nanoparticles (e.g., from nickel [19, 32, 33] and platinum [34]), with nitrophenyl [35–37], and with carboxylic

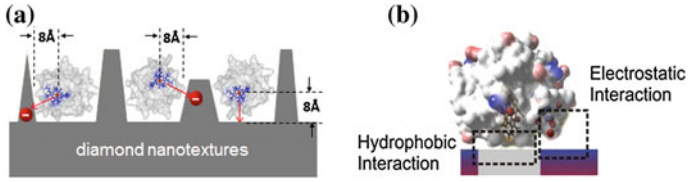

Fig. 4 Schematic demonstration of **a** trapping of cytochrome c using diamond nanotextures for an efficient electron transfer process and **b** the interaction of cytochrome c with the OH-terminated diamond surface [26, 30]

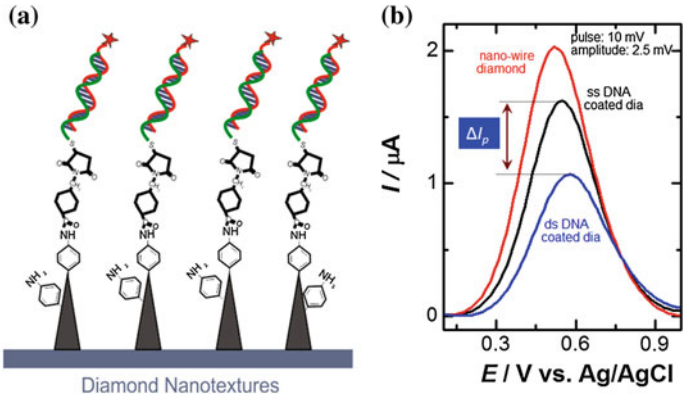

Fig. 5 **a** Schematic plots of the tip-functionalization of diamond nanotextures for DNA immobilization and **b** differential pulse voltammetric detection of DNA hybridization on diamond nanotexures using negatively charged redox mediators [35, 36]

acid-terminated poly(pyrrole) [38] were applied to construct electrochemical [19], DNA biosensors [35–37, 39], and immunosensors [32, 33, 38].

For example, tip coating of diamond nanowires with nickel nanoparticles improved the detection limit for glucose detection to 10 μM [19]. Non-enzymatic oxidation of glucose and electrocatalytic oxidation of methanol have been reported on diamond nanotextures decorated with platinum nanoparticles [34]. Diamond nanotextures were functionalized via electrochemical grafting at −0.05 V (vs. Ag/Ag^+) for 4 s with 1.0 mM diazonium salts. The density of phenyl molecules at diamond nanotextures was about 2×10^{13} cm^{-2} [36]. Constant-current mode scanning tunneling microscope (STM) conducted before and after grafting with nitrophenyl on diamond textures indicated the preferential bonding of nitrophenyl to the tips of wires [13]. Such tip-functionalized diamond nanotextures were applied to immobilize DNA with aid of SSMCC chemistry, as shown in Fig. 5a [35, 36]. Electrochemical detection of DNA hybridization on such an interface was realized by use of negatively charged redox indicators [35, 36]. Figure 5b shows the differential pulse voltammograms of $Fe(CN)_6^{3-/4-}$ on diamond nanotextures based electrode before and after functionalized with single-strand DNA (ss DNA) and double-strand DNA (ds DNA). The difference of peak currents of redox indicators on these interfaces was applied to detect DNA hybridization. A detection limit of about 2 pM was realized on 0.03 cm^2 sensor area over 30 hybridization/denaturation cycles. The discrimination of single-base mismatched complementary DNA was achieved [35–37, 39].

Furthermore, several diamond nanowires based immunosensors have been reported [33, 34, 38]. For instance, biotinylated anti-IgG was specifically linked to nickel particles. The charger transfer resistance, detected from electrochemical impedance spectroscopy, was linear with IgG concentration in the range of 0.3–400 ng mL^{-1}. The detection limit of IgG was found to be 0.3 ng mL^{-1} [33].

2.3.2 Electrochemical Capacitors

Diamond nanowires [42–50, 133, 134, 139] and porous diamond films [51–53] have been utilized extensively for supercapacitors construction, although the capacitance of a smooth diamond electrode itself is not so huge, in comparison with other non-carbon electrodes. Moreover, up to the electrolyte applied, boron-doping level, and the surface morphology as well as terminations, the capacitance of a diamond electrode varies greatly. For a nanocrystalline diamond electrode with a boron-doping level of 5×10^{20} cm^{-3}, its double-layer capacitance is about 3.6–7, 14–20, 11–15 μF cm^{-2} in aqueous, organic, and ionic liquid solution, respectively. However due to enhanced surface areas as well as the wide working potential windows [42, 43] (ca. 2.5 V in aqueous electrolytes and 7.3 V in organic electrolytes [44–46]), diamond nanostructures are very promising for supercapacitors construction. Taking diamond networks as an example, a diamond network with a porosity from 15 to 68 % led to hundreds of times enhancement of the surface areas than that of flat diamonds (e.g., 490-fold for a 3 μm thick diamond network).

Electric double layer capacitors (EDLCs) based on diamond honeycomb nanostructures showed a capacitance of 3910 μF cm^{-2} and 666 μF cm^{-2} in aqueous and organic solution, respectively [44–46]. Diamond foam based EDLCs attained specific capacitances of 598 and 436 μF cm^{-2} in aqueous and organic solutions, respectively. A high power density of 807 W cm^{-3} was achieved, which touched the best power performance of electrolytic capacitors [47]. In 0.1 M H_2SO_4, the double layer capacitance of a diamond network was calculated to be 13.7 F g^{-1} or 17.3 F cm^{-3} at a scan rate of 0.1 V s^{-1} [48]. Figure 6a compares the capacitive behaviour of a smooth diamond electrode with two diamond networks in 0.1 M H_2SO_4 [48]. Silicon nanowires coated with a thin diamond film (240 nm in thickness) was employed for EDLCs application. The capacitance of such an EDLC was 105 μF cm^{-2} in a mixture

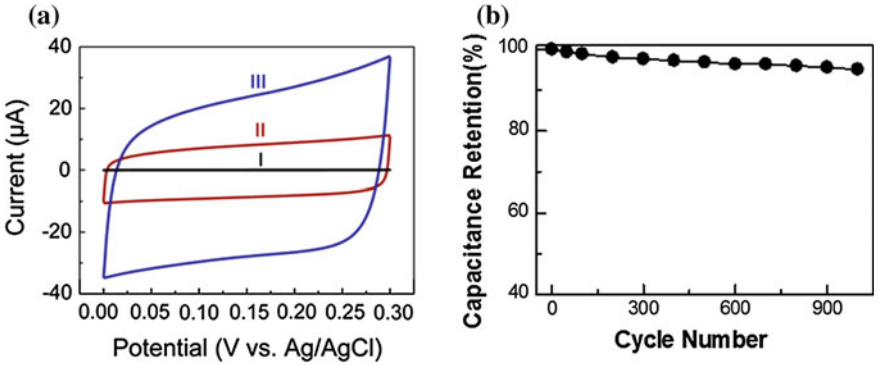

Fig. 6 Cyclic voltammograms of **a** flat diamond film (I), diamond network-1 (II) and diamond network-2 (III) in 0.1 M H_2SO_4 at a scan rate of 0.1 V s^{-1}; **b** Capacitance retention of a diamond EDLC as a function of charge/discharge cycles, tested in 1.0 M Na_2SO_4 at a scan rate of 0.1 V s^{-1} [43, 48]

of propylene carbonate with 1-methyl-1-propylpyrrolidinium bis(trifluoromethylsulfonyl)imide, one room temperature ionic liquid. A high energy density of 84 μJ cm^{-2} and power density of 0.94 mW cm^{-2} and good stability (retention stability of 93.3 % after 10,000 cycles at a scan rate of 5 V s^{-1}) were achieved [49]. Figure 6b presents a very recent retention stability test result for a diamond EDLC in 1.0 M Na_2SO_4 [43]. Only 5 % reduction of the capacitance is seen. This is due to high chemical stability of diamond electrodes in any kind of media as well as at different working potentials. On TiO_2 nanotubes coated with boron-doped diamond (200–500 nm in thickness), the specific capacitance is dependent on the boron concentration. In 0.1 M $NaNO_3$, the specific capacitance of 2.10, 4.79, and 7.46 mF cm^{-2} was obtained at a scan rate of 0.01 V s^{-1} for a [B]/[C] ratio of 2000, 5000 and 10,000, respectively. The substantial improvement of electrochemical performance and the excellent rate capability was explained with the synergistic effect of TiO_2 treatment in CH_4:H_2 plasma and the high electrical conductivity of boron-doped diamond layers [50]. Recently, "diamond paper" showed in aqueous electrolyte a capacitance of 0.688 mF cm^{-2} per layer, or 0.645 F g^{-1}. The specific power of these diamond based supercapacitors reached 1×10^5 W kg^{-1} [134].

Other porous diamond films/membranes [51–53] have been employed for supercapacitor applications. For example, a two-step thermal treatment method was developed for the fabrication of porous conductive boron-doped diamond films [51]. The sizes of the pores were from several tens to several hundred nanometer. Such a porous membrane exhibited a double-layer capacitance of ca. 140 μF cm^{-2} in an aqueous electrolyte, estimated from cyclic voltammetry and galvanostatic measurements [52]. Porous boron-doped diamond films overgrew on CNTs, showed c.a. 450 times greater electroactive areas and double-layer capacitance values than those for the equivalent flat boron-doped diamond electrodes [51]. Another porous diamond, based on the overgrowth of a highly porous polypyrrole scaffold with a thin boron-doped diamond film, exhibited remarkable electrochemical properties, including a large double layer capacitance up to 3 mF cm^{-2} in aqueous $LiClO_4$ and a low electrochemical impedance [53].

Diamond nanowires were coated as well with nickel hydroxide [133] to construct diamond pseudocapacitors. Although much higher capacitances of diamond pseudocapacitors than those of diamond EDLCs were obtained, the big shortcoming of diamond pseudocapacitors is the poor retention stability of their capacitances. This results from low stability of pseudo or redox-active species on diamond electrode surface (e.g., these metal oxides are easily stripped from diamond during the charging/discharging processes) [43, 133].

2.3.3 Other Applications

Diamond nanostructures have been proposed as well for other electrochemical applications [40, 54–56, 135, 138]. For example, porous diamond membrane was applied as a filter to separate differently charged 5-carboxyfluorescein and substance P under different biases [55]. Diamond nanowires was also applied to enhance the

intensity of electrogenerated chemiluminescence (ECL) of a ruthenium tris(2,2′) bipyridyl/tripropylamine system [40]. Owing to their superior properties (e.g., large surface areas, improved electrocatalytic activities, and accelerated electron transfer rates), the enhancement of ECL intensity was attributed mainly to the highly facile oxidation of tripropylamine on diamond nanowires. This study revealed an effective method for the ultrasensitive detection of ruthenium tris(2,2′)bipyridyl. It will help to increase the efficiency of immunoassays and DNA analysis based on ruthenium tris (2,2′)bipyridyl electrogenerated chemiluminescence. Diamond nanowires have been utilized as well for electrocatalytic applications [135, 138]. For example, diamond nanowires coated with Pt have been applied for electrocatalytic hydrogen evolution [135]. Very recently, electrochemical CO_2 reduction has been achieved on diamond coated silicon nanowires, where doped diamond acts as a metal-free electrocatalyst [138]. Recently, diamond foams composed of hollow spheres of polycrystalline boron-doped diamond have been chemically modified with two donor–acceptor type molecular dyes and further utilized as electrode materials for p-type dye-sensitized solar cells in an aqueous electrolyte solution containing methyl viologen as a redox mediator [141].

3 Diamond Nanoparticles

3.1 Synthesis Methods

3.1.1 Un-doped Diamond Nanoparticles

Un-doped diamond nanoparticles with size down to 20 nm have been produced via ball-milling of micro-sized high-pressure-high-temperature (HPHT) diamond films. In this way, diamond nanoparticles less than 10 nm were seldomly obtained. With the aid of bead-assisted sonic disintegration, the production of diamond nanoparticles 70–80 nm in diameter was realized by milling polycrystalline chemical-vapor-deposited (CVD) diamond films. These nanoparticles have faceted shapes with sharp edges, which correspond to fractured crystallographic planes. Using such a method, few spherical nanoparticles were found. Another more widely applied approach to produce spherical diamond nanoparticles these days is to use dynamic processes from molecules of explosives and different graphite precursors [5, 57], including the direct transformation of graphite by an external shock wave, the detonation of graphite mixed with explosive, and the detonation of high energy explosive. Diamond nanoparticles synthesized from these detonation methods have a core of sp^3 diamond with a size of 4–5 nm and a shell of a mixture of sp^2 and sp^3 carbon as well as oxygen based functional groups (e.g., carboxylic acids, esters, lactones, etc.) [5, 57].

3.1.2 Doped Diamond Nanoparticles

Doped diamond particles, mainly boron-doped diamond particles, have been obtained mainly via the overgrowth of insulating diamond particles with boron-doped diamond, solid-state diffusion, and milling [119, 120]. For example, boron-doped diamond powder was synthesized under HPHT using B-doped graphite intercalation compositions as carbon sources [121]. Recently, Kruger et al. [123] applied a multistep milling process followed by purification and surface oxidation to produce 10–60 nm boron-doped diamond nanoparticles. The starting material used for such a milling process was heavily boron-doped diamond films.

3.2 Electrochemical Properties

To investigate electrochemistry of diamond nanoparticles, diamond nanoparticles are always treated and/or cleaned. The applied processes include acid boiling, oxidation by Osswald method, plasma treatment, thermal annealing, etc. For example, surface treatment of diamond nanoparticles by heating in air and in a hydrogen flow results in oxygenated (O-) and hydrogenated (H-) nanoparticles, respectively. The acid boiling removes effectively the responses associated with sp^2 carbon impurities. On these diamond nanoparticles based film electrodes, a potential independent capacitive signal has been obtained and checked by recording their cyclic voltammograms in solutions without any redox species [67].

Diamond nanoparticles based film electrodes have been fabricated with various techniques [129], such as drop coating from their ethanol suspensions, smearing a mineral oil paste of diamond nanoparticles, grinding diamond powders into the tip of a Pt wire sealed in a small pipette, electrophoretically deposition, co-deposition, non-contact microprinting, and layer-by-layer self-assembly by a high pressure/high-temperature methodology, etc.

3.2.1 Un-doped Diamond Nanoparticles

Diamond nanoparticles, one form of un-doped diamond, showed different electrochemical properties from un-doped bulk diamond. They are surprisingly electrochemically active. Their electrochemical activities depend greatly on the nature/type (e.g., detonation, HPHT particles), surface terminals, as well as the pH value of the solutions.

Detonation Diamond Nanoparticles

Novoselova et al. [58] studied for the first time the redox activity of diamond powders based film electrode in aqueous electrolytes. Redox couples of

$[Fe(CN)_6]^{3-/4-}$ and $Ce^{3+/4+}$ were applied as the probes. The voltammetric response of $Fe(CN)_6^{3-/4-}$ was however superimposed on a linearly sloping background and with small peak currents. The reduction currents were two times larger than the oxidation currents. In the case of the $Ce^{3+/4+}$ redox couple, additional current responses were noted, besides the expected current peaks. Zang et al. [59] used cavity electrodes to investigate redox activities of diamond nanoparticles. Stable background currents in KCl electrolyte over a wide potential range (−1.2 to 2.0 V vs. Ag/AgCl) and a quasi-reversible reversible electrode reaction for the $Fe(CN)_6^{3-/4-}$ couple with the electrode reaction rate constant of 2.87×10^{-3} cm s^{-1} were obtained. The recorded AC impedance spectra were consistent with those obtained on a porous electrode [59].

Holt and her colleague [60–65] made extensive investigation on the electrochemistry of detonation diamond nanoparticles. Differential pulse voltammetry of electrode-immobilised layers of diamond nanoparticles in the absence of solution redox species revealed oxidation and reduction peaks, resulting from direct electron transfer reactions of diamond nanoparticles themselves [60]. Moreover, the presence of detonation diamond nanoparticles on the (diamond) electrode modified the cyclic voltammetric response of $Fe(CN)_6^{3-/4-}$ and $IrCl_6^{3-/2-}$ when the scan rate was slow and the concentration of redox couples was low. For example, enhancements of oxidation currents were noted at potentials where the oxidation of the surface of diamond nanoparticles started. The enhancements of reduction currents were likewise observed where diamond nanoparticle was reducible [60]. Attenuated total reflectance infrared spectroscopy was then used to monitor spectral features of the surface of diamond nanoparticles [61]. Aqueous $IrCl_6^{2-}$ was added in these studies. They found that electron transfer between the surface of diamond nanoparticle and the solution redox species results in the oxidation of 8.5 % of surface alcohol groups, with concomitant formation of unsaturated ketone or quinone-like moieties [61]. Scanning electrochemical microscopy (SECM) [62] was applied as well to investigate the redox behavior of detonation diamond nanoparticles based film electrode (Fig. 7). Different collection modes and various redox mediators were

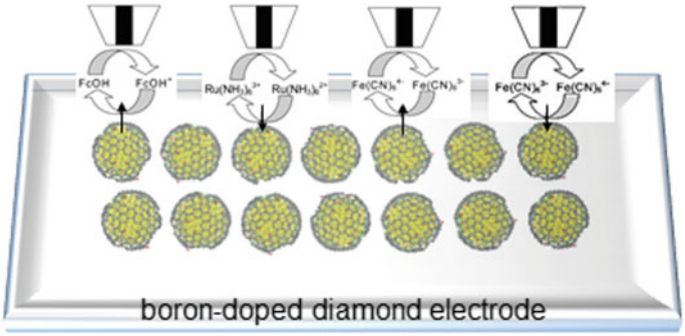

Fig. 7 Schematic illustration of SECM investigation of redox activities of diamond nanoparticles based film electrode with different redox probes and collection modes [62]

used to estimate quantitatively heterogeneous rate constants and overpotentials of redox probes. On such an electrode, extremely sluggish kinetics were found for all redox couples, but the reduction of $Fe(CN)_6^{3-}$ was found to be especially slow when compared to the oxidation of $Fe(CN)_6^{4-}$. Overall, the rate constants were about 10 times faster at diamond nanoparticles based film electrode than that on the boron-doped diamond film [62]. Supported with in-situ infrared (IR) experimental results, they stated that electron transfer at the diamond nanoparticle surface takes place at similar sites as on the boron-doped diamond film. But the reaction sites are present at higher relative concentrations due to the higher surface to bulk atom ratio of the nanoparticles. The modification of an electrode with an immobilised layer of diamond nanoparticles was found later to enhance significantly the redox currents for reversible oxidation of ferrocene methanol. Current enhancement is dependence of the diameter of diamond nanoparticles, with enhancement increasing in the order 1000 nm < 250 nm < 100 nm < 10 nm < 5 nm [64].

To explain such the 'molecule-like' redox behaviour of diamond nanoparticles, Holt et al. proposed a so-called feedback mechanism [60–64]. Figure 8 shows schematically such a mechanism. A self-conducted oxidation and reduction process via surface states at specific potentials triggers the redox activities of diamond nanoparticles. The magnitude of current enhancement depends on the standard potential of the redox couple relative to those of the surface states of diamond nanoparticles. Provided that at the nanoscale surface properties of diamond nanoparticles dominate over those of the bulk, electron transfer occurs between these essentially insulating particles and a redox species in solution or an underlying electrode. The occurrence of reversible reduction of diamond nanoparticles via electron injection into available surface states at well-defined reduction potentials is thus speculated. In this process, diamond nanoparticles act as a source and a sink of electrons for the promotion of solution redox reactions [67]. They then concluded that the electrochemical activity of un-doped diamond nanoparticles is attributed to unsaturated bonding at the diamond nanoparticle surface [60]. Electron transfer occurs between electroactive species generated at the underlying electrode during voltammetry and the immobilized diamond nanoparticles in the interfacial region, leading to regeneration of the starting species and hence enhancement in currents.

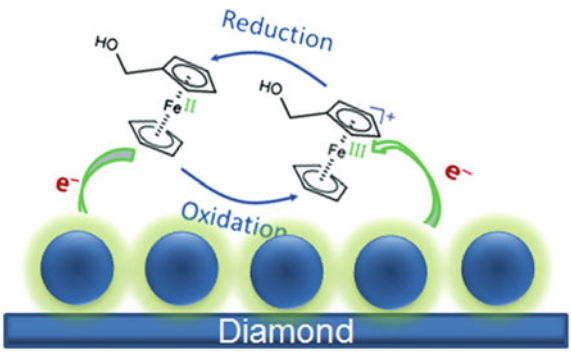

Fig. 8 Schematic plot of a catalytic feedback mechanism: catalytic reactions of ferrocene methanol on diamond nanoparticles based film electrode [60]

Moreover, electrochemical activity of detonation diamond nanoparticles (5 nm in diameter) based film electrode was tunable via surface functionalizations and graphitization degree of diamond nanoparticles. For example, both redox reactions of $Fe(CN)_6^{3-/4-}$ and $Fe^{3+/2+}$ were quasi-reversible on the pristine diamond nanoparticles based film electrodes. The O-terminated diamond nanoparticles exhibited the greatest electrochemical activity for the redox couples $Ru(NH_3)_6^{3+/2+}$ and $Fe(CN)_6^{4-/3-}$ while the H-terminated diamond nanoparticles the least. After fluorination of diamond nanoparticles, the electrode reactions of $Fe(CN)_6^{3-/4-}$ became slower, while the amino modification accelerated the electron transfer process of $Fe(CN)_6^{3-/4-}$ anions but slowed the redox reaction of $Fe^{3+/2+}$ cations [69]. Annealing of diamond nanoparticles in vacuum led to the variation of electrochemical activities of diamond nanoparticles. The electron transfer rate of the $Fe(CN)_6^{3-/4-}$ redox couple in aqueous solutions decreased with an increase of the annealing temperature. Re-annealing in air restored the original electrochemical activity. This is because vacuum annealing below 850 °C removed parts of the oxygen-containing surface functionalities from the surface of diamond nanoparticles and produced more sp^2 carbon atoms in the shell. When the annealing temperature was at 900–1100 °C, more serious graphitization produced a continuous fullerenic shell wrapped around a diamond core, which had a high conductivity and electrochemical activity [68].

Furthermore, electrochemical activity of detonation diamond nanoparticles based film electrode was found to be affected by pH values of the solution, namely the by solution proton concentration [60, 62]. In the solutions with pH value of 4 and 5, well-defined peaks in the potential range of −0.1 to 0.5 V (vs. Ag/AgCl) were seen from differential pulse voltammograms. As the solution pH increased, they became much smaller in magnitude and far less resolved [60, 62]. This is because the electrochemical response of diamond nanoparticles based film electrode resulted from the oxidation and reduction of surface states of diamond nanoparticles. The potentials of these surface states are however pH-dependent; moreover they are able to interact with solution redox species [60, 62].

HPHT Diamond Nanoparticles

Fermin et al. [66, 67] combined zeta potential measurements in the solutions and electrochemical studies in thin-layer assemblies of diamond nanoparticles to investigate electrochemical properties of undoped HPHT diamond particles. The estimated point-of-zero zeta potential was 6.6. The zeta potentials of these nanoparticles depended on pH. They found that in a single electron transfer process 1×10^4 redox centres per particle were involved. Electrochemical signals were rather sensitive to the extent of sp^2 hybridisation at the surface of diamond powders [66]. Electrochemical field-effect transistors were employed to investigate the charge transport properties of O- and H-terminated diamond particles in the presence and absence of metal nanostructures [67]. The assembly of H-terminated diamond particle was characterized by a charging process at a potential above 0.1 V

(vs. Ag/AgCl). The responses were found to be associated with hole-injection into the valence band edge, which is shifted to approximately −4.75 eV (vs. vacuum) upon hydrogenation. The position of the valence band edge as well as hole number density at the H-terminated diamond particle surface varied as a function of the applied potential [70]. Through the discussion in terms of the electrochemical formation of charge carriers in the diamond particles, percolation theory, and charge screening at the double layer, Fermin et al. suggested that charge transport on un-doped diamond particles is not only determined by the intrinsic surface conductivity of individual diamond particles, but also by particle-to-particle charge transfer [71]. The latter contribution effectively controls the assembly conductivity in the presence of an electrolyte solution as the difference between hydrogenated and oxygenated particles vanishes. The conductivity in the presence of metal nanoparticles is mainly determined by the metal volume fraction, while diamond surface termination and the presence of electrolyte solutions exert only minor effects [71].

3.2.2 Doped Diamond Nanoparticles

To check electrochemical activities of boron-doped diamond particles, redox probes of $Fe(CN)_6^{3-/4-}$ and $Ru(NH_3)_6^{3+/2+}$ and a polytetrafluoroethylene binder were used. These particles were produced via microwave plasma-assisted CVD growth of a thin boron-doped layer on insulating diamond powders (8–12 μm in diameter). At scan rates between 10 and 500 mV s^{-1}, the peak difference of the anodic wave from the cathodic wave was high (in the range 0.14–0.35 V vs. Ag/AgCl) for both redox probes, suggesting significant ohmic resistance within the powder/binder electrode [119]. Later the same technique was applied to overgrow small-sized diamond powders (100 and 500 nm in diameter). Both powders had increased conductivities. Well-defined electrochemical responses were obtained on these powders based film electrode for the redox reactions of $Fe(CN)_6^{3-/4-}$, $Ir(Cl)_6^{2-/3-}$, and $Fe^{2+/3+}$, in comparable to typical responses shown on the high-quality, boron-doped nanocrystalline diamond thin-film [120]. Later the electrochemical characteristics of boron-doped diamond powders based film electrodes were investigated by measuring the cyclic voltammetric curves and AC impedance spectra [121]. The powders were synthesized under HPHT using B-doped graphite intercalation compositions as carbon sources. For the $Fe(CN)_6^{3-/4-}$ redox couple, the electrode reaction process is reversible or quasi-reversible at the scan rates of 0.01–1.0 V s^{-1}. At the low scan rates the linear relation between peak current and square root of scan rate indicates that the electrode process is a diffusion-controlled mass-transport process. The electrochemical behavior is similar to a planar electrode. With an increase of the scan rate the electrode process is controlled by the mass transport plus kinetic process. AC impedance spectra exhibited the porous structure characteristic of boron-doped diamond powders based film electrode [121]. The boron-doped diamond nanoparticles made by solid-state diffusion method showed a lower capacitance but a higher conductivity than undoped

diamond nanoparticles [122]. In the potential range of −0.3 to 1.8 V (vs. SCE), a featureless voltammetric response was obtained. Recently high quality boron-doped diamond nanoparticles with a size of 10–60 nm and a boron concentration of approximately 2.3×10^{21} cm^{-3} have been produced by Kruger et al. [123]. However the electrochemistry of those nanoparticles has not been reported yet.

3.3 Electrochemical Applications

3.3.1 Un-doped Diamond Nanoparticles

Electroanalytical Applications

Due to the features of giant specific surface areas and large numbers of surface defects as well as the cluster structure, detonation diamond nanoparticles have increased electrical conductivities. As a novel type of electrode materials, they have been employed frequently for electrochemical and biochemical sensing applications [72–86].

Many electrochemical sensors based on diamond nanoparticles have been reported, including the sensors for the detection of azathioprine [72], epinephrine and uric acid in the presence of ascorbic acid [73], nitrite [74], tryptophan, and 5-hydroxytryptophan [75]. The matrix of diamond and silver nanoparticles were applied for electrochemical monitoring of thioridazine [76] and hydrogen peroxide [77]. For example, on an electrode based on a chitosan matrix and the mixture of nanographite and diamond nanoparticles, electrocatalytic detection of azathioprine was realized in a concentration range from 0.2 to 100 μM with a detection limit of 65 nM [72]. The same electrode was applied successfully to detect epinephrine (0.01–10 μM) and uric acid (0.01–60 μM) in the presence of ascorbic acid. The detection limit was 3 nM for both epinephrine and uric acid [73]. Voltammetric monitoring of 30 nM tryptophan and 6 nM 5-hydroxytryptophan was shown to be possible on diamond nanoparticles based film electrode [75]. By decorating diamond nanoparticles with silver nanoparticles, voltammetric determination of thioridazine was achieved in the concentration range of 0.08–100 μM with a detection limit of 0.01 μM [76]. Synergistic effect of two kinds of nanoparticles was proposed to demonstrate the satisfactory electrochemical activity [76]. Such a matrix was applied to fabricate a non-enzymatic hydrogen peroxide sensor [77]. On such a sensor, hydrogen peroxide was detected in the range of 0.1–34.0 μM with a detection limit of 0.01 μM and a sensitivity of 1.59×10^6 μA M^{-1} [77]. TiO_2 nanoparticles coated diamond nanoparticles exhibited higher electrochemical activity than the pristine diamond nanoparticles, especially higher catalytic ability towards the oxidation of nitrite anions. A detection limit of 0.55 μM and a linear range of 0.05–1.0 mM for the detection of nitrite ions were achieved [78].

Diamond nanoparticles based electrochemical biosensors have been reported. Glucose oxide, cytochrome c, hemoglobin, horseradish peroxidase, alcohol

dehydrogenase, and lactate oxidase have been immobilized on diamond nanoparticles for the detection of glucose [79–83], and alcohols [84], lactate [85], respectively. For example, alcohol dehydrogenase (ADH) has been adsorbed on oxidized diamond nanoparticles. The adsorption of the non-covalently immobilized ADH, estimated with Langmuir isotherms, was dependent on pH values of the solutions. A higher packing density was achieved at the isoelectric point of ADH. Its relative activity was retained up to 70 % under optimum pH conditions. An ethanol bioelectrochemical cell and an alcohol biosensor were then proposed [84]. On the diamond nanoparticles and polyaniline based electrode, direct electrochemistry of cytochrome c was achieved, leading to electrocatalytic detection of nitrite ions in a concentration range from 0.5 μM to 3 mM with a detection limit of 0.16 μM [81]. Diamond nanoparticles and porous poly(aniline)–poly(2-acrylamido 2-methyl propane sulfonic acid) network based sponges were prepared to entrap horseradish peroxidase [83]. On such a matrix, electrocatalytic reduction of hydrogen peroxide was realized in a concentration range of 1–45 mM with a rapid response time of 5 s, a high sensitivity of 129.6 μA M^{-1} and a low detection limit of 59 μM [83]. An electrochemical biosensor based on diamond nanoparticles was proposed as well for lactate determination. The workable concentration range was from 50 μM to 0.7 mM, the sensitivity was 4.0 μA mM^{-1}, and the detection limit was 15 μM [85]. Antibody immobilization was reported on diamond nanoparticles seeded inter-digitated electrodes (IDEs). Such an impedance biosensor improved the overall detection sensitivity, namely the resistance to charge transfer. The sensor performance was better than those based on gold or ITO electrodes. When sensing bacteria from 106 cfu mL^{-1} *E. coli* O157:H7, the resistance to charge transfer at the IDEs decreased by 38.8 %, which is nearly 1.5 times better than that reported previously using redox probes. Further in the case of 108 cfu mL^{-1} *E. coli* O157:H7, the charge transfer resistance changed by 46 % [86].

Electrocatalysts

Different kinds of diamond nanoparticles (e.g., surface graphitized diamond nanoparticles with a diamond core covered by a graphitic carbon shell, bucky diamond nanoparticles with a nanoscale diamond core surrounded by a fullerene shell, and graphene coated diamond nanoparticles) have been used as the support to load catalysts (e.g., Pt [87–93], Ni [94, 95], Ti [96], Pd [97], Pt/Ni [98], Pt/Ru [99–102], Sn/Pb [103], Pt/Eu [91, 99], and metal oxides [104–106]). The mostly investigated electrocatalytic reactions include electrocatalytic oxidation of methanol/formic acid/CO as well as oxygen reduction reaction. To load these catalysts on diamond nanoparticles, numerous approaches have been developed, including electrodeposition [88, 92], chemical reduction [93], and microwave-assisted polyol synthesis [91, 99]. For example, electrodeposition of Pt nanoparticles on un-doped diamond nanoparticles (5–100 nm in diameter) were conducted in 1.1 mM chloroplatinic acid solution. The electrodeposited Pt nanoparticles were well-dispersed on the facet surfaces of diamond nanoparticles [88, 107]. Pt and Ru

nanoparticles were chemically deposited on un-doped and boron-doped diamond nanoparticles through the use of $NaBH_4$ as reducing agent and sodium dodecyl benzene sulfonate as a surfactant [93]. Microwave-assisted reduction method [91, 98] has been used for the preparation of catalysts of Pt [91], Pt/Ni [98], and Pt/Ru [102] on the surface of diamond nanoparticles. A microwave heating polyol method was used to prepare the Pt/Ru electrocatalyst on the surface of un-doped diamond nanoparticles. It was found that Ru was partly dissolved in the face-centered cubic Pt lattice. The Pt/Ru nanoparticles were small and uniform with the size of 2–4 nm, and highly dispersed on the surface of diamond nanoparticles [102]. A simple ultrasonic treatment in the presence of diamond powders prior to electrodeposition improved spatial distribution and a higher Pt dispersion over the electrode [99–102]. A two-step method was reported to modify diamond nanoparticles with Pt and TiO_2 nanoparticles, namely first by a microwave hydrolysis step, and then electrodeposition of Pt nanoparticles [104–106].

For the first time Fermin et al. [97] utilized Pd and HPHT diamond nanoparticles (500 nm in diameter) based electrocatalysts for the electrochemical stripping of CO and oxidation of formic acid in the acid solutions. Later the same group studied the electrocatalytic reactivity of Pt nanoparticles coated HPHT diamond particles towards the oxidation of adsorbed CO, methanol, and formic acid with differential electrochemical mass spectrometry. Diamond nanoparticles with different surface terminations were used for these electrocatalytic oxidation reactions, leading to different oxidation mechanisms [89]. Towards the ability of the electrocatalytic oxidation of methanol, diamond nanoparticles with smaller diameters (e.g., 5 nm) exhibited better electrocatalytic activity than bigger ones (e.g., 100 nm) after the surface of diamond nanoparticles were coated with electrodeposited Pt nanoparticles [88, 107]. The application of these Pt modified diamond electrodes in the electrochemical oxidation of hydrogen peroxide was demonstrated [92]. The ink-paste method was used to prepare the membrane electrode assembled with Pt and Pt/Ru modified un-doped and boron-doped diamond nanoparticle catalytic systems [100]. Their performances were examined in a direct methanol fuel cell system [100]. The Pt/Ru catalyst exhibited higher activity and stability for methanol electrooxidation reaction than individual Pt catalyst [102]. The investigation of electrocatalytic reduction of oxygen on metal catalysts coated diamond nanoparticles has been conducted further using cyclic voltammetry, chronoamperometry and linear sweep voltammetry [98]. The Pt/Ni catalysts exhibited better electrocatalytic activities than the Pt catalysts either for methanol oxidation reaction or for oxygen reduction reaction [98]. In the acid medium the Pt/TiO_2 catalyst system possessed higher electrocatalytic activity for methanol oxidation reaction compared with the individual Pt catalyst [96]. TiN coated diamond nanoparticles showed higher catalytic activity and better stability in methanol oxidation and oxygen reduction reactions compared with the individual catalysts on carbon and on diamond nanoparticles [106].

Energy Storage

Diamond nanoparticles have been employed as the electrode material for energy storage, such as for electrochemical capacitors [108–113, 136], lithium batteries [114, 115], and dye-sensitive solar cells [116]. For supercapacitors, diamond nanoparticles are always thermally annealed at the temperatures above 1000 °C. Due to the generation of carbon onions, the energy is possible to be stored under a high current density and a high capacitance.

For example, Gogotsi et al. investigated and compared in organic and aqueous electrolytes the performance of EDLCs based on carbon onions, diamond nanoparticles, carbon black and multi-walled carbon nanotubes [108]. Different methods were applied, including galvanostatic cycling, electrochemical impedance spectroscopy and cyclic voltammetry. To construct pseudocapacitors, the surface of diamond nanoparticles and carbon onions was coated with a layer of phosphomolybdate [111] or polyanilline [112, 113] (produced via electropolymerization in a cavity electrode or a chemical oxidation approach [113]). Carbon onions and phosphomolybdate based pseudocapacitance exhibited a 20 % increase in the capacitance (up to 600 mF cm^{-2} at 5 V s^{-1}) [111]. Due to the porous network structure [113], the pseudocapacitance based on diamond nanoparticles and polyaniline (with the weight ratios of 3–28 %) increased to 640 F g^{-1} in 1.0 M H_2SO_4. This capacitance was 3–4 times higher than that of the activated carbons and more than 15 times higher than that of diamond nanoparticles and carbon onions. Moreover the charge-discharge characteristics were stable for 10,000 cycles [113].

Some experiments to use diamond nanoparticles for lithium batteries were reported as well [114, 115]. For example, a volumetric capacity of less than 23 mA h cm^{-3} has been shown, although it was much lower than 450–700 mA h cm^{-3} offered by state-of-the-art high-density cathodes used in commercial Li-ion batteries [115]. The composite system of polyaniline and diamond nanoparticles prepared via electrochemical polymerization techniques was applied toward the iodine/iodide redox couple for the construction of dye-sensitised solar cells [116].

Other Applications

Diamond nanoparticles have been applied as corrosion inhibition [117], and as the metal-free catalysts for oxidant- and steam-free dehydrogenation [118, 140]. For example, the nanocomposite of polyaniline and diamond nanoparticles showed an ohmic junction and wide potential values, independent of redox characteristics of both polyaniline and diamond nanoparticles. This is due to its chain conformation and electronic properties (achieved by the interaction of the free electron pairs of the nitrogen atoms in the polyaniline with a charged molecule on the surface of diamond nanoparticles), leading to excellent corrosion inhibitor characteristics [117].

3.3.2 Doped Diamond Particles

Boron-doped diamond powders based film electrodes were shown to be dimensionally stable at 1.4 V (vs. Ag/AgCl) for 1 h in 0.5 M H_2SO_4 at 80 °C. They are thus corrosion-resistant during anodic polarization. In contrast, glassy carbon powders polarized under identical conditions underwent significant microstructural degradation and corrosion [124]. Electrocatalytic oxidation of methanol was tested on the composite based on boron-doped diamond particles (500 nm and 5 μm in diameter) and metallic oxides [125]. By coating boron-doped diamond nanoparticles with $Ni(OH)_2$, a non-enzymatic glucose sensor was constructed. The detection limit for glucose detection was 1.2 μM [126]. Recently, boron-doped diamond nanoparticles have been electrostatically self-assembled on carbon nanotubes. Such a 3D network showed a low electron transfer resistance but a large effective surface area, resulted in an improved electrochemical performance in glucose detection [128]. The construction of electrochemical capacitors using RuO_2 coated diamond powders has been reported as well [127].

4 Diamond Nanoelectrode Arrays

Small-dimensional electrodes (e.g., nanoelectrodes) offer various benefits over planar macroscopic electrodes [10, 142, 143], such as reduced Ohmic resistance, enhanced mass transport, decreased charging currents, decreased deleterious effects of solution resistance, and high possibility for fast voltammetric measurements. However, single nanoelectrode only generates a small current that is relatively difficult to detect with conventional electrochemical setups. This has been circumvented by fabricating nanoelectrode arrays or ensembles that operate in parallel. They amplify the signal of individual nanoelectrodes but do not lose their beneficial characteristics. If diamond nanoelectrode arrays or ensembles are applied for sensor applications, their performances with respect to the sensitivity, detection limit, life time, and reproducibility, will be highly improved [10, 130, 142, 143]. This is because boron-doped diamond is one of the most appropriate and optimized material for the fabrication of these arrays and ensembles [6, 137]. Moreover, since a macroscopic diamond electrode shows a higher degree of inhomogeneity with respect to boron-doping level and termination effects due to its macroscopic dimensions, one would thus expect a homogenized behavior on a diamond nanoelectrode array (NEA) or nanoelectrode ensemble (NEE) [131, 132]. This is due to the small grains of diamond films as well as a more effective termination of these small electrochemical active areas.

4.1 Production Procedures

NEAs and NEEs were fabricated using E-beam lithography and nanosphere lithography, respectively [131]. The following is the fabrication steps of NEAs [131]. On a 200 nm thin boron-doped nanocrystalline diamond film, a 200 nm thick SiO_2 is deposited. This oxide layer is structured using E-beam lithography with subsequent nickel deposition and SF_6 etching of SiO_2. In the next step, metal contacts are deposited using photolithography to allow electrical contact for electrochemical characterization. In the crucial step, a 140 nm thin insulating nanocrystalline diamond film is grown on the part of the boron-doped nanocrystalline diamond layer that is exposed to the CVD plasma and not protected by SiO_2 islands. With the removal of SiO_2 in hydrofluoric acid, the arrays of recessed boron-doped nanocrystalline diamond nanoelectrodes surrounded by insulating diamond (NEAs) are obtained. In the NEAs we fabricated the nanoelectrodes are distributed in a hexagonal order, having a well-defined radius of 250 nm and a distance of 10 µm next to other nanoelectrodes and an electrode density of 11×10^5 cm^{-2}. One SEM image of such a NEA is shown in Fig. 9a.

Nanosphere lithography was developed to fabricate NEEs [131]. Initially, a photolithography step is used to deposit metal contacts on diamond. Thereafter, the sample is immersed in a solution of SiO_2 spheres. The next step involves the growth of insulating diamond around the above mentioned spheres. Insulating diamond selectively grows on the area exposed to the plasma. After the removal of SiO_2 spheres in hydrofluoric acid, nanoelectrodes having a concave shape are fabricated. These nanoelectrodes thus have the same size as the diameter of SiO_2 spheres. Since the concentration of the SiO_2 solution is directly correlated to the density of spheres on the diamond surface as well as to the average distance of neighboring spheres, the density of those nanoelectrodes are controllable. The size of the nanoelectrodes can be well-defined by selecting market-available SO_2 spheres as

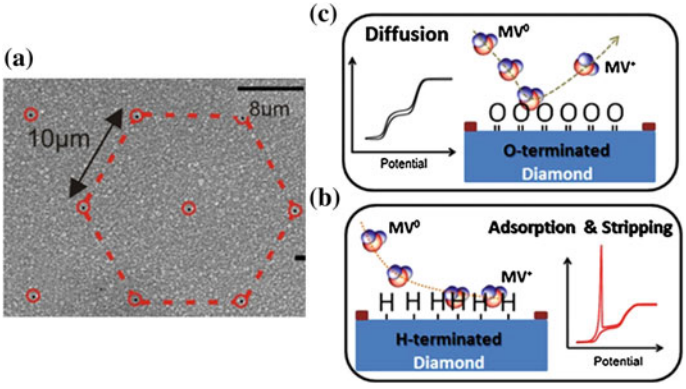

Fig. 9 **a** SEM image of a diamond NEA; Schematic plots of volumetric behavior of methyl viologen on **b** H- and **c** O-terminated diamond NEAs, respectively [131, 132]

required. For example, to obtain sigmoidal voltammograms, we chose a SiO_2 concentration of 9.55×10^8 cm^{-3}, corresponding to a surface density of 9.7×10^5 cm^{-2} and an average distance of neighboring spheres of ~ 10 μm. The size of the nanoelectrodes in a NEE is about 175 nm. The density of nanoelectrodes is about 8.5×10^5 cm^{-2} [131].

4.2 Electrochemical Properties

Cyclic voltammetry of $Fe(CN)_6^{3-/4-}$, $Ru(NH_3)_6^{2+/3+}$ and $IrCl_6^{2-/3-}$ were conducted on the NEA and NEE in 0.1 M KCl solution. The scan rates were varied from few mV s^{-1} up to 10 V s^{-1}. At small scan rates (e.g., 20 mV s^{-1} for the NEA and 1 mV s^{-1} for the NEE), the voltammograms have mixed shapes, indicating partially overlapping diffusion hemispheres. Increasing the scan rates leads to typical steady-state sigmoidal voltammograms on both electrodes. The change is more distinct on the NEA than on the NEE [131]. Impedance was performed on the NEA and NEE in 0.1 M KCl at open circuit potentials. The redox couple of $Fe(CN)_6^{3-/4-}$ (1.0 mM) was added. Their impedance spectra have similar characteristics, exhibiting a large semicircle in the high-frequency regime and at low frequencies a transition to linear diffusion with unity slope (particularly observable for the NEA) [131]. A semicircle at high frequency regime is due to a three-dimensional hemispherical diffusion on the diamond NEA and NEE [144–146]. The transition at low frequencies represents the regime of overlapping diffusion hemispheres. These behaviors are similar with those obtained from voltammetry [131].

Moreover, the voltammetric response of $Ru(NH_3)_6^{2+/3+}$ and $IrCl_6^{2-/3-}$ on a diamond NEA show the dependence of surface termination on the charge of the analytes [131]. Please note that on planar macroscopic diamond electrodes both analytes show no dependence of electron transfer rate constants on the surface termination of diamond electrodes. On the H-terminated diamond NEAs, the voltammogram of the anion $IrCl_6^{2-/3-}$ shows a fast electron transfer while at the O-terminated surface, the steady-state current as well as the slope of the transition from reduction to oxidation decreases, indicative of a slower electron transfer. This tendency is similar for another negatively charged redox couple of $Fe(CN)_6^{3-/4-}$. However, the opposite effect is observed for the positively charged redox molecules $Ru(NH_3)_6^{2+/3+}$. That is, on an O-terminated diamond NEA, the electron transfer rate for $Ru(NH_3)_6^{2+/3+}$ is faster than that on a H-terminated surface. It is known that H-terminated diamond surface has a positive surface dipole layer ("positive" refers to the interface of diamond to the liquid) and the O-terminated surface results in a negative surface dipole layer. Such behaviors are therefore probably due to either an electrostatic or a site blocking effect [131].

4.3 Electrochemical Applications

Diamond NEAs have been applied for electrochemical sensing [130] and the investigation of surface-sensitive adsorption phenomena [132]. The adsorption of neutral methyl viologen (MV^0) was used as a model system. Diffusion-controlled processes manifest themselves as sigmoidal-shaped voltammograms on O-terminated diamond NEAs, whereas adsorption-controlled processes result in peaks in the voltammogram for H-terminated diamond NEAs. The change in the shapes of these voltammograms is due to the drastic changes that occur in the diffusion profiles during the transition. It alters from hemispherical diffusion on the O-terminated surface to thin-layer electrochemistry upon the adsorption on the H-terminated surface. In this way the de-convolution of diffusion-controlled current from adsorption-controlled current was conducted. By analysing anodic stripping process at high scan rates, the deposition of amorphous MV^0 was approved on H-terminated diamond NEAs. These results are schematically shown in Fig. 9b, c for H- and O-terminated diamond NEAs, respectively [132]. The types and the concentration of the buffer solutions were changed to alter the interaction of MV^0 with H-terminated diamond NEAs [132]. Increasing urea concentrations leads to the same impact on the adsorption of MV^0 as guanidine, which weakens hydrophobic interaction. This effect of ions on the interaction of MV^0 and the hydrophobic diamond surface is correlated with the Hofmeister series [132]. Subsequently, the adsorption of MV^0 on H-terminated diamond NEAs is controlled by hydrophobic interaction [132]. Therefore diamond NEA is ideal for the study of adsorption phenomena at the liquid-solid interface in voltammetry [132].

5 Summary and Outlook

Electrochemistry using diamond nanostructures, nanoparticles, nanoelectrodes, in other words, diamond nanoelectrochemistry, has been paid much attention in the fields of electrochemical sensors, energy, and electrocatalysts during the past years. In such electrochemical systems, nanostructured diamond (e.g., textures, wires, pores, nanoelectrodes, etc.) and diamond nanoparticles were used as the working electrode, instead of macro-sized diamond bulk electrode. From fundamental aspects of diamond nanoelectrochemistry, future activities should focus on the effect of surface termination of diamond at the nanoscale, diamond-to-graphite ratios, surface defects, and morphology (e.g., size, shape, etc.) effects of diamond nanostructures on their electrochemical properties in the absence and presence of redox probes. Coating these diamond nanostructures and nanoparticles with stable and electroactive modifiers is important for their applications for sensors, energy storage and conversion, and catalytic reactions. Doping diamond nanostructures and nanoparticles with dopants such as N and other atoms will widen their applications such as for electrocalaytic reactions (e.g., oxygen reduction/evolution

reaction, CO_2 reduction reaction, etc.). Combination of diamond nanostructures with diamond nanoparticles, or the formation of their hybrid nanocomposites, for example, diamond nanowires based diamond nanoelectrodes, diamond nanoparticles coated diamond nanoelectrodes, will take full advantages of diamond as well as nanoelectrochemistry, leading to more novel concepts and applications [147, 148]. For example, on such hybrid nanocomposites, the investigation of diamond electrochemistry and electroanalysis at the nanoscale (e.g., capacitive current at a single nanowire, single molecule detection, etc.), which is hard to be realized on other electrode materials, will be feasible.

In conclusion, progress and achievements on electrochemistry using diamond nanostructures, nanoparticles and nanoelectrodes are summarized. Through the input from material scientists, chemists, physics, and engineers, more and nicer results in the fields of electrochemical properties and applications of diamond nanostructures and nanoparticles will be obtained in coming years. By showing and comparing the results published in literature, we believe this chapter will help the readers to know more how electrochemistry of diamond nanostructures and nanoparticles started as well as where and how it goes in future.

Acknowledgements The authors thank the financial support from German Research Foundation (DFG) under the project (YA344/1-1).

References

1. M. Iwaki, S. Sato, K. Takahashi, H. Sakairi, Electrical conductivity of nitrogen and argon implanted diamond. Nucl. Instrum. Methods Phys. Res. **209–210**, 1129 (1983). doi:10.1016/0167-5087(83)90930-4
2. Y.V. Pleskov, A.Y. Sakharova, M.D. Krotova, L.L. Bouilov, B.V. Spitsyn, Photoelectrochemical properties of semiconductor diamond. J. Electroanal. Chem. **228**, 19 (1987). doi:10.1016/0022-0728(87)80093-1
3. A. Fujishima, Y. Einaga, T.N. Rao, D.A. Tryk (eds.), *Diamond Electrochemistry* (Elsevier, Tokyo, 2005)
4. R.L. McCreery, Advanced carbon electrode materials for molecular electrochemistry. Chem. Rev. **108**, 2646–2687 (2008). doi:10.1021/cr068076m
5. E. Brillas, C.A. Martinez-Huitle (eds.), *Synthetic Diamond Films: Preparation, Electrochemistry, Characterization, and Applications* (Wiley, 2011)
6. N. Yang (ed.), *Novel Aspects of Diamond* (Springer, 2014)
7. N. Yang, W. Smirnov, C.E. Nebel, Diamond nanotextures: technologies, properties, and electrochemical applications, M. Chehimi, J. Pinson (eds.), *Applied Surface Chemistry of Nanomaterials* (NOVA Publisher, 2013), pp 33–54
8. Y. Yu, L. Wu, J. Zhi, Diamond nanowires: fabrication, structure, properties, and applications. Angew. Chem. Int. Ed. **53**(2014), 14326–14351 (2013). doi:10.1002/anie.10803
9. S. Szunerits, Y. Coffinier, R. Boukherroub, Diamond nanowires: a novel platform for electrochemistry and matrix-free mass spectrometry. Sensors **15**, 12573–12593 (2015). doi:10.3390/s150612573
10. R.W. Murray, Nanoelectrochemistry: metal nanoparticles, nanoelectrodes, and nanopores. Chem. Rev. **108**, 2688–2720 (2008). doi:10.1021/cr068077e
11. J.D. Wadhawan, R.G. Compton (eds.), *Electrochemistry*, vol. 11, (RSC Publisher, 2012)

12. M.V. Mirkin, S. Amemiya (eds.), *Nanoelectrochemistry*, (CRC Press, 2015)
13. N. Yang, H. Uetsuka, E. Osawa, C.E. Nebel, Vertically aligned nanowires from boron-doped diamond. Nano Lett. **8**, 3572–3576 (2008). doi:10.1021/nl801136h
14. W. Smirnov, A. Kriele, N. Yang, C.E. Nebel, Aligned diamond nano-wires: fabrication and characterisation for advanced applications in bio and electrochemistry. Diam. Relat. Mater. **18**, 186–189 (2009). doi:10.1016/j.diamond.2009.09.001
15. Y.S. Zou, Y. Yang, Y.L. Zhou, Z.X. Li, H. Yang, B. He, I. Bello, W.J. Zhang, Surface nanostructuring of boron-doped diamond films and their electrochemical performance. J. Nanosci. Nanotech. **11**, 7914–7919 (2011). doi:10.1016/j.diamond.2003.10.066
16. M. Wei, C. Terashima, M. Lv, A. Fujishima, Z.-Z. Gu, Boron-doped diamond nanograss array for electrochemical sensors. Chem. Commun. 3624–3626 (2009). doi:10.1039/B903284C
17. J. Shalini, K.J. Sankaran, C.L. Dong, C.Y. Lee, N.H. Tai, I.N. Lin, In situ detection of dopamine using nitrogen incorporated diamond nanowire electrode. Nanoscale **5**, 1159–1167 (2013). doi:10.1039/C2NR32939E
18. D. Luo, L. Wu, J. Zhi, Fabrication of boron-doped diamond nanorod forest electrodes and their application in nonenzymatic amperometric glucose sensing. ACS Nano **3**, 2121–2128 (2009). doi:10.1021/nn9003154
19. Q. Wang, P. Subramanian, M. Li, W.S. Yeap, K. Haenen, Y. Coffinier, R. Boukherroub, S. Szunerits, Non-enzymatic glucose sensing on long and short diamond nanowires electrodes. Electrochem. Commun. **34**, 286–290 (2013). doi:10.1016/j.elecom.2013.07.014
20. N. Yang, W. Smirnov, C.E. Nebel, Three-dimensional electrochemical reactions on tip-coated diamond nanowires with nickel nanoparticles. Electrochem. Commun. **27**, 89–91 (2013). doi:10.1016/j.elecom.2012.10.044
21. S. Szunerits, Y. Coffinier, E. Galopin, J. Brenner, R. Boukherroub, Preparation of boron-doped diamond nanowires and their application for sensitive electrochemical detection of tryptophan. Electrochem. Commun. **12**, 438–441 (2010). doi:10.1016/j.elecom.2010.01.014
22. Q. Wang, A. Vasilescu, P. Subramanian, A. Vezeanu, V. Andrei, Y. Coffinier, M. Li, R. Boukherroub, S. Szunerits, Simultaneous electrochemical detection of tryptophan and tyrosine using boron-doped diamond and diamond nanowires electrodes. Electrochem. Commun. **35**, 84–87 (2013). doi:10.1016/j.elecom.2013.08.010
23. M. Lv, M. Wei, F. Rong, C. Terashima, A. Fujishima, Z.-Z. Gu, Electrochemical detection of catechol based on as-grown and nanograss array boron-doped diamond electrodes. Electroanalysis **22**, 199–203 (2010). doi:10.1002/elan.200900296
24. N. Yang, R. Hoffmann, W. Smirnov, A. Kriele, C.E. Nebel, Interface properties of cytochrome c on nano-textured diamond surface. Diam. Relat. Mater. **20**, 269–273 (2011). doi:10.1016/j.diamond.2010.12.012
25. N. Yang, W. Smirnov, A. Kriele, R. Hoffmann, C.E. Nebel, Nano-textured surface for enhanced protein redox activity. Phys. Status Solidi A **207**, 2069–2072 (2010). doi:10.1002/pssa.201000085
26. N. Yang, R. Hoffmann, W. Smirnov, A. Kriele, C.E. Nebel, Direct electrochemistry of cytochrome c on nano-textured diamond surface. Electrochem. Commun. **12**, 1218–1221 (2010). doi:10.1016/j.elecom.2010.06.023
27. W. Wu, L. Bai, X. Lin, Z. Tang, Z.-Z. Gu, Nanograss array boron-doped diamond electrode for enhanced electron transfer from Shewanella loihica PV-4. Electrochem. Commun. **13**, 872–874 (2011). doi:10.1016/j.elecom.2011.05.025
28. W. Wu, Z.-Z. Gu, X. Liu, L. Bai, Z. Tang, Nanograss array boron-doped diamond electrode for toxicity sensor with Shewanella loihica PV-4 in bioelectrochemical systems. Sens. Lett. **12**, 191–196 (2014). doi:10.1166/sl.2014.3272
29. R. Hoffmann, A. Kriele, S. Kopta, W. Smirnov, N. Yang, C.E. Nebel, Intentional adsorption of cytochrome c to diamond. Phys. Status Solidi A **207**, 2073–2077 (2010). doi:10.1002/pssa.201000043

30. R. Hoffmann, A. Kriele, H. Obloh, N. Tokuda, W. Smirnov, N. Yang, C.E. Nebel, The creation of a biomimetic interface between boron-doped diamond and immobilized proteins. Biomaterials **30**, 7325–7332 (2011). doi:10.1016/j.biomaterials.2011.06.052
31. R. Hoffmann, H. Obloh, N. Tokuda, N. Yang, C.E. Nebel, Fractional surface termination of diamond by electrochemical oxidation. Langmuir **28**, 47–50 (2012). doi:10.1021/la2039366
32. P. Subramanian, J. Foord, D. Steinmueller, Y. Coffinier, R. Boukherroub, S. Szunerits, Diamond nanowires decorated with metallic nanoparticles: a novel electrical interface for the immobilization of histidinylated biomolecules. Electrochim. Acta **110**, 4–8 (2013). doi:10.1016/j.electacta.2012.11.010
33. P. Subramanian, A. Motorina, W.S. Yeap, K. Haenen, Y. Coffinier, V. Zaitsev, J. Niedziolka-Jonsson, R. Boukherroub, S. Szunerits, Impedimetric immunosensor based on diamond nanowires decorated with nickel nanoparticles. Analyst **139**, 1726–1731 (2014). doi:10.1039/C3AN02045B
34. I. Shpilevaya, W. Smirnov, S. Hirsz, N. Yang, C.E. Nebel, J.S. Foord, Nanostructured diamond decorated with Pt particles: preparation and electrochemistry. RSC Adv. **4**, 531–537 (2014). doi:10.1039/C3RA43763A
35. N. Yang, H. Uetsuka, E. Osawa, C.E. Nebel, Vertically aligned diamond nanowires for DNA sensing. Angew. Chem. Int. Ed. **47**, 5183–5185 (2008). doi:10.1002/anie.200801706
36. N. Yang, H. Uetsuka, C.E. Nebel, Biofunctionalization of vertically aligned diamond nanowires. Adv. Funct. Mater. **19**, 887–893 (2009). doi:10.1002/adfm.200990018
37. N. Yang, H. Uetsuka, O.A. Williams, E. Osawa, N. Tokuda, C.E. Nebel, Vertically aligned diamond nanowires: Fabrication, characterization, and application for DNA sensing. Phys. Stat. Sol. A **206**, 2048–2056 (2009). doi:10.1002/pssa.200982222
38. P. Subramanian, I. Mazurenko, Y. Coffinier, Y. Zaitsev, R. Boukherroub, S. Szunerits, Diamond nanowires modified with poly[3-(pyrrolyl)carboxylic acid] for the immobilization of histidine-tagged peptides. Analyst **139**, 4343–4349 (2014). doi:10.1039/C4AN00146J
39. C.E. Nebel, N. Yang, H. Uetsuka, E. Osawa, N. Tokuda, O. Williams, Diamond nano-wires, a new approach towards next generation electrochemical gene sensor platforms. Diam. Relat. Mater. **18**, 910–917 (2009). doi:10.1016/j.diamond.2008.11.024
40. Y. Yang, J.-W. Oh, Y.-R. Kim, C. Terashima, A. Fujishima, J.S. Kim, H. Kim, Enhanced electrogenerated chemiluminescence of a ruthenium tris(2,2′)bipyridyl/tripropylamine system on a boron-doped diamond nanograss array. Chem. Commun. **46**, 5793–5795 (2010). doi:10.1039/C0CC00773K
41. N. Yang, W. Smirnov, C.E. Nebel, Fabrication, properties and electrochemical applications of diamond nanostructures. MRS Proceedings **1511**, mrsf12-1511-ee07-01. doi:10.1557/opl.2012.1661
42. V.D. van Wyk, P.G.L. Baker, T. Waryo, E.I. Iwuoha, C. O'Sullivan, Electrochemical evaluation of a novel boron doped diamond (BDD) material for application as potential electrochemical capacitor. Anal. Lett. **44**, 2005–2018 (2011). doi:10.1080/00032719.2010.539735
43. S. Yu, N. Yang, H. Zhuang, J. Meyer, S. Mandal, O.A. Williams, I. Lilge, H. Schönherr, X. Jiang, Electrochemical supercapacitors from diamond. J. Phys. Chem. C **33**, 18918–18926 (2015). doi:10.1021/acs.jpcc.5b04719
44. K. Honda, T.N. Rao, D.A. Tryk, A. Fujishima, M. Watanabe, K. Yasui, H. Masuda, Electrochemical characterization of the nanoporous honeycomb diamond electrode as an electrical double-layer capacitor. J. Electrochem. Soc. **147**, 659–664 (2000). doi:10.1149/1.1393249
45. K. Honda, T.N. Rao, D.A. Tryk, A. Fujishima, M. Watanabe, K. Yasui, H. Masuda, Impedance characteristics of the nanoporous honeycomb diamond electrodes for electrical double-layer capacitor applications. J. Electrochem. Soc. **148**, A668–A679 (2001). doi:10.1149/1.1373450
46. M. Yoshimura, K. Honda, R. Uchikado, T. Kondo, T.N. Rao, D.A. Tryk, A. Fujishima, Y. Sakamoto, K. Yasui, H. Masuda, Electrochemical characterization of nanoporous

honeycomb diamond electrodes in non-aqueous electrolytes. Diam. Relat. Mater. **10**, 620–626 (2001). doi:10.1016/S0925-9635(00)00381-2
47. F. Gao, M. Wolfer, C.E. Nebel, Highly porous diamond foam as a thin-film micro-supercapacitor material. Carbon **80**, 833–840 (2014). doi:10.1016/j.carbon.2014.09.007
48. H. Zhuang, N. Yang, H. Fu, L. Zhang, C. Wang, N. Huang, X. Jiang, Diamond network: template-free fabrication and properties. ACS Appl. Mater. Interfaces **7**, 5384–5390 (2015). doi:10.1021/am508851r
49. F. Gao, G. Lewes-Malandrakis, M. Wolfer, W. Müller-Sebert, P. Gentile, D. Aradilla, T. Schubert, C.E. Nebel, Diamond-coated silicon wires for supercapacitor applications in ionic liquids. Diam. Relat. Mater. **51**, 1–6 (2015). doi:10.1016/j.diamond.2014.10.009
50. K. Siuzdak, R. Bogdanowicz, M. Sawczak M. Sobaszek, Enhanced capacitance of composite TiO_2 nanotube/boron-doped diamond electrodes studied by impedance spectroscopy. Nanoscale **7**, 551–558 (2015). doi:10.1039/C4NR04417G
51. H. Zanin, P.W. May, D.J. Fermin, D. Plana, S.M.C. Vieira, W.I. Milne, E.J. Corat, Porous boron-doped diamond/carbon nanotube electrodes. ACS Appl. Mater. Interfaces **6**, 990–995 (2014). doi:10.1021/am4044344
52. T. Kondo, Y. Kodama, S. Ikezoe, K. Yajima, T. Aikawa, M. Yuasa, Porous boron-doped diamond electrodes fabricated via two-step thermal treatment. Carbon **77**, 783–789 (2014). doi:10.1016/j.carbon.2014.05.082
53. C. Hebert, E. Scorsone, M. Mermoux, P. Bergonzo, Porous diamond with high electrochemical performance. Carbon **90**, 102–109 (2015). doi:10.1016/j.carbon.2015.04.016
54. H. Kato, J. Hees, R. Hoffmann, M. Wolfer, N. Yang, S. Yamasaki, C.E. Nebel, Diamond foam electrodes for electrochemical applications. Electrochem. Commun. **33**, 88–91 (2013). doi:10.1016/j.elecom.2013.04.028
55. F. Gao, C. Giese, G. Lewes-Malandrakis, C.E. Nebel, Porous diamond membrane fabricated by templated growth for electrochemical separation processes*, 2015 ECS Meeting Abstract, 213-A*
56. S. Ruffinatto, H.A. Girard, F. Becher, J.C. Arnault, D. Tromson, P. Bergonzo, Diamond porous membranes: A material toward analytical chemistry. Diam. Relat. Mater. **55**, 123–130 (2015). doi:10.1016/j.diamond.2015.03.008
57. O.A. Williams (ed.), *Nanodiamond* (RSC Publisher, 2014)
58. I.A. Novoselova, E.N. Fedoryshena, E.V. Panov, A.A. Bochechka, L.A. Romanko, Electrochemical properties of compacts of nano-and microdisperse diamond powders in aqueous electrolytes. Phys. Solid State **46**, 748–750 (2004). doi:10.1134/1.1711465
59. J.B. Zang, Y.H. Wang, S.Z. Zhoa, L.Y. Bian, J. Lu, Electrochemical properties of nanodiamond powder electrodes. Diam. Relat. Mater. **16**, 16–20 (2007). doi:10.1016/j.diamond.2006.03.010
60. K.B. holt, Undoped diamond nanoparticles: origins of surface redox chemistry. Phys. Chem. Chem. Phys. **12**, 2048–2058 (2010). doi:10.1039/B920075D
61. J. Scholz, A.J. McQuillan, K.B. Holt, Redox transformations at nanodiamond surfaces revealed by in situ infrared spectroscopy. Chem. Commu. **47**, 12140–12142 (2011). doi:10.1039/C1CC14961J
62. K.B. Holt, C. Ziegler, J. Zang, J. Hu, J.S. Foord, Scanning electrochemical microscopy studies of redox processes at undoped nanodiamond surfaces. J. Phys. Chem. C **113**, 2761–2770 (2009). doi:10.1021/jp8038384
63. K.B. Holt, D.J. Caruana, E.J. Millan-Barrios, Electrochemistry of undoped diamond nanoparticles: accessing surface redox states. J. Am. Chem. Soc. **131**, 11272–11273 (2009). doi:10.1021/ja902216n
64. K.B. Holt, C. Ziegler, D.J. Caruana, J. Zang, E.J. Millan-Barrios, J. Hu, J.S. Foord, Redox properties of undoped 5 nm diamond nanoparticles. Phys. Chem. Chem. Phys. **10**, 303–310 (2008). doi:10.1039/B711049
65. A.T.S. Varley, M. Hirani, G. Harrison, K.B. Holt, Nanodiamond surface redox chemistry: influence of physicochemical properties on catalytic processes. Faraday Discuss. **172**, 349–364 (2014). doi:10.1039/C4FD00041B

66. W. hongthani, D.J. Fermin, Layer-by-layer assembly and redox properties of undoped HPHT diamond particles. Diam. Relat. Mater. **19**, 680–684 (2010). doi:10.1016/j.diamond.2010.01.039
67. D. Plana, J.J.L. Humphrey, K.A. Bradley, V. Celorrio, D.J. Fermin, Charge transport across high surface area metal/diamond nanostructured composites. ACS Appl. Mater. Interfaces **5**, 2985–2990 (2013). doi:10.1021/am302397p
68. J. Zang, Y. Wang, L. Bian, J. Zhang, F. Meng, Y. Zhao, S. Ren, X. Qu, Surface modification and electrochemical behaviour of undoped nanodiamonds. Electrochim. Acta **72**, 68–73 (2012). doi:10.1016/j.electacta.2012.03.169
69. Y. Wang, H. Huang, J. Zang, F. Meng, L. Dong, J. Su, Electrochemical behavior of fluorinated and aminated nanodiamond. Int. J. Electrochem. Sci. **7**, 6807–6815 (2012)
70. W. Hongthani, N.A. Fox, D.J. Fermin, Electrochemical properties of two dimensional assemblies of insulating diamond particles. Langmuir **27**, 5112–5118 (2011). doi:10.1021/la1045833
71. D. Plana, J.J.L. Humphrey, K.A. Bradley, V. Celorrio, D.J. Fermin, Charge transport across high surface area metal/diamond nanostructured composites. ACS Appl. Mater. Interfaces **5**, 2985–2990 (2013). doi:10.1021/am302397p
72. S. Shahrokhian, M. Ghalkhani, Glassy carbon electrodes modified with a film of nanodiamond–graphite/chitosan: application to the highly sensitive electrochemical determination of azathioprine. Electrochim. Acta **55**, 3621–3627 (2010). doi:10.1016/j.electacta.2010.01.099
73. S. Shahrokhian, M. Khafaji, Application of pyrolytic graphite modified with nano-diamond/graphite film for simultaneous voltammetric determination of epinephrine and uric acid in the presence of ascorbic acid. Electrochim. Acta **55**, 9090–9096 (2010). doi:10.1016/j.electacta.2010.08.043
74. L.H. Chen, J.B. Zang, Y.H. Wang, L.Y. Bian, Electrochemical oxidation of nitrite on nanodiamond powder electrode. Electrochim. Acta **53**, 3442–3445 (2008). doi:10.1016/j.electacta.2007.12.023
75. S. Shahrokhian, M. Bayat, Pyrolytic graphite electrode modified with a thin film of a graphite/diamond nano-mixture for highly sensitive voltammetric determination of tryptophan and 5-hydroxytryptophan. Microchim. Acta **174**, 361–366 (2011). doi:10.1007/s00604-011-0631-2
76. S. Shahrokhian, N.H. Nassab, Nanodiamond decorated with silver nanoparticles as a sensitive film modifier in a jeweled electrochemical sensor: application to voltammetric determination of thioridazine. Electroanalysis **25**, 417–425 (2013). doi:10.1002/elan.201200339
77. B. Habibi, M. Jahanbakhshi, Sensitive determination of hydrogen peroxide based on a novel nonenzymatic electrochemical sensor: silver nanoparticles decorated on nanodiamonds. J. Iran. Chem. Soc. **12**, 1431–1438 (2015). doi:10.1007/s13738-015-0611-2
78. L.Y. Bian, Y.H. Wang, J. Lu, J.B. Zang, Synthesis and electrochemical properties of TiO_2/nanodiamond nanocomposite. Diam. Relat. Mater. **19**, 1178–1182 (2010). doi:10.1016/j.diamond.2010.05.007
79. W. Zhao, J.J. Xu, Q.Q. Qiu, H.Y. Chen, Nanocrystalline diamond modified gold electrode for glucose biosensing. Biosens. Bioelectron. **22**, 649–655 (2006). doi:10.1016/j.bios.2006.01.026
80. M. Briones, E. Casero, M.D. Petit-Dominguez, M.A. Ruiz, A.M. Parra-Alfambra, F. Pariente, E. Lorenzo, L. Vazquez, Diamond nanoparticles based biosensors for efficient glucose and lactate determination. Biosens. Bioelectron. **68**, 521–528 (2015). doi:10.1016/j.bios.2015.01.044
81. A.I. Gopalan, K.-P. Lee, S. Komathi, Bioelectrocatalytic determination of nitrite ions based on polyaniline grafted nanodiamond. Biosens. Bioelectron. **26**, 1638–1643 (2010). doi:10.1016/j.bios.2010.08.042

82. J.-T. Zhu, C.-G. Shi, J.-J. Xu, H.-Y. Chen, Direct electrochemistry and electrocatalysis of hemoglobin on undoped nanocrystalline diamond modified glassy carbon electrode. Bioelectrochemistry **71**, 243–248 (2007). doi:10.1016/j.bioelechem.2007.07.002
83. A.I. Gopalan, S. Komathi, G.S. Anand, K.P. Lee, Nanodiamond based sponges with entrapped enzyme: a novel electrochemical probe for hydrogen peroxide. Biosens. Bioelectron. **46**, 136–141 (2013). doi:10.1016/j.bios.2013.02.036
84. E. Nicolau, J. Mendez, J.J. Fonseca, K. Griebenow, C.R. Cabrera, Bioelectrochemistry of non-covalent immobilized alcohol dehydrogenase on oxidized diamond nanoparticles. Bioelectrochemistry **85**, 1–6 (2012). doi:10.1016/j.bioelechem.2011.11.002
85. M. Briones, E. Casero, M.D. Petit-Dominguez, M.A. Ruiz, A.M. Parra-Alfambra, F. Pariente, E. Lorenzo, L. Vazquez, Diamond nanoparticles based biosensors for efficient glucose and lactate determination. Biosens. Bioelectron. **68**, 521–528 (2015). doi:10.1016/j.bios.2015.01.044
86. W.L. Zhang, K. Patel, A. Schexnider, S. Banu, A.D. Radadia, Nanostructuring of biosensing electrodes with nanodiamonds for antibody immobilization. ACS Nano **8**, 1419–1428 (2014). doi:10.1021/nn405240g
87. L.Y. Bian, Y.H. Wang, J.B. Zang, F.W. Meng, Y.L. Zhao, Detonation-synthesized nanodiamond as a stable support of Pt electrocatalyst for methanol electrooxidation. Int. J. Electrochem. Sci. **7**, 7295–7303 (2012)
88. L. Bian, Y. Wang, J. Zang, J. Yu, H. Huang, Electrodeposition of Pt nanoparticles on undoped nanodiamond powder for methanol oxidation electrocatalysts. J. Electroanal. Chem. **644**, 85–88 (2010). doi:10.1016/j.jelechem.2010.04.001
89. V. Celorrio, D. Plana, J. Florez-Montano, M.G. Montes de Oca, A. Moore, M.J. Lazaro, E. Pastor, D.J. Fermin, Methanol oxidation at diamond-supported Pt nanoparticles: effect of the diamond surface termination. J. Phys. Chem. C **117**, 21735–21742 (2013). doi:10.1021/jp4039804
90. J. Zang, Y. Wang, L. Bian, J. Zhang, F. Meng, Y. Zhao, R. Lu, X. Qu, S. Ren, Graphene growth on nanodiamond as a support for a Pt electrocatalyst in methanol electro-oxidation. Carbon **50**, 3032–3038 (2012). doi:10.1016/j.carbon.2012.02.089
91. J. Zang, Y. Wang, L. Bian, J. Zhang, F. Meng, Y. Zhao, X. Qu, S. Ren, Bucky diamond produced by annealing nanodiamond as a support of Pt electrocatalyst for methanol electrooxidation. Int. J. Hydrogen Energy **37**, 6349–6355 (2012). doi:10.1016/j.ijhydene.2012.01.034
92. J. Hu, X. Lu, J.S. Foord, Nanodiamond pretreatment for the modification of diamond electrodes by platinum nanoparticles. Electrochem. Comm. **12**, 676–679 (2010). doi:10.1016/j.elecom.2010.03.004
93. L. La-Torre-Riveros, R. Guzman-Blas, A.E. Mendez-Torres, M. Prelas, D.A. Tryk, C.R. Cabrera, Diamond nanoparticles as a support for Pt and PtRu catalysts for direct methanol fuel cells. ACS Appl. Mater. Interface **4**, 1134–1147 (2012). doi:10.1021/am2018628
94. E.A. Levashov, P.V. Vakaev, E.I. Zamulaeva, A.E. Kudryashov, V.V. Kurbatkina, D.V. Shtansky, A.A. Voevodin, A. Sanz, Disperse-strengthening by nanoparticles advanced tribological coatings and electrode materials for their deposition. Surf. Coat. Technol. **201**, 6176–6181 (2007). doi:10.1016/j.surfcoat.2006.08.134
95. L.-N. Tsai, G.-R. Shen, Y.-T. Cheng, W. Hsu, Performance improvement of an electrothermal microactuator fabricated using Ni-diamond nanocomposite. J. Microelectromech. Syst. **15**, 149–158(2006). doi:10.1109/JMEMS.2005.863737
96. Y. Wang, Y. Zhao, R. Lu, L. Dong, J. Zang, J. Lu, X. Xu, Nano titania modified nanodiamonds as stable electrocatalyst supports for direct methanol fuel cells. J. Electrochem. Soc. **162**, F211–F215 (2015). doi:10.1149/2.0051503jes
97. A. Moore, V. Celorrio, M.M. de Oca, D. Plana, W. Hongthani, M.J. Lazaro, D.J. Fermin, Insulating diamond particles as substrate for Pd electrocatalysts. Chem. Commun. **47**, 7656–7658 (2011). doi:10.1039/c1cc12387d

98. Y. Wang, J. Zang, L. Dong, H. Pan, Y. Yuan, Y. Wang, Graphitized nanodiamond supporting PtNi alloy as stable anodic and cathodic electrocatalysts for direct methanol fuel cell. Electrochim. Acta **113**, 583–590 (2013). doi:10.1016/j.electacta.2013.09.091
99. X. Lu, J.-P. Hu, J.S. Foord, Q. Wang, Electrochemical deposition of Pt-Ru on diamond electrodes for the electrooxidation of methanol. J. Electroanal. Chem. **654**, 38–43 (2011). doi:10.1016/j.jelechem.2011.01.034
100. L. La-Torre-Riveros, R. Guzman-Blas, A.E. Mendez-Torres, M. Prelas, D.A. Tryk, C.R. Cabrera, Diamond nanoparticles as a support for Pt and Pt-Ru catalysts for direct methanol fuel cells. ACS Appl. Mater. Interfaces **4**, 1134–1147 (2012). doi:10.1021/am2018628
101. L. La-Torre-Riveros, E. Abel-Tatis, A.E. Mendez-Torres, D.A. Tryk, M. Prelas, C.R. Cabrera, Synthesis of platinum and platinum-ruthenium-modified diamond nanoparticles. J. Nanopart. Res. **13**, 2997–3009 (2011). doi:10.1007/s11051-010-0196-8
102. R. Lu, J. Zang, Y. Wang, Y. Zhao, Microwave synthesis and properties of nanodiamond supported PtRu electrocatalyst for methanol oxidation. Electrochim. Acta **60**, 329–333 (2012). doi:10.1016/j.electacta.2011.11.068
103. T. Fujimura, V.Y. Dolmatov, G.K. Burkat, E.A. Orlova, M.V. Veretennikova, Electrochemical codeposition of Sn–Pb–metal alloy along with detonation synthesis nanodiamonds. Diam. Relat. Mater. **13**, 2226–2229 (2004). doi:10.1016/j.diamond.2004.06.009
104. G.R. Salazar-Banda, K.I.B. Eguiluz, L.A. Avaca, Boron-doped diamond powder as catalyst support for fuel cell applications. Electrochem. Commun. **9**, 59–64 (2006). doi:10.1016/j.elecom.2006.08.038
105. L.Y. Bian, Y.H. Wang, J. Lu, J.B. Zang, Synthesis and electrochemical properties of TiO_2/nanodiamond nanocomposite. Diam. Relat. Mater. **19**, 1178–1182 (2010). doi:10.1016/j.diamond.2010.05.007
106. Y. Zhao, Y. Wang, L. Dong, J. Huang, J. Zang, J. Lu, X. Xu, Core-shell structural nanodiamond@TiN supported Pt nanoparticles as a highly efficient and stable electrocatalyst for direct methanol fuel cells. Electrochim. Acta **148**, 8–14 (2014). doi:10.1016/j.electacta.2014.10.024
107. L.Y. Bian, Y.H. Wang, J.B. Zang, F.W. Meng, Y.L. Zhao, Microwave synthesis and characterization of Pt nanoparticles supported on undoped nanodiamond for methanol electrooxidation. Int. J. Hydrogen Energy **37**, 1220–1225 (2012). doi:10.1016/j.ijhydene.2011.09.118
108. C. Portet, G. Yushin, Y. Gogotsi, Electrochemical performance of carbon onions, nanodiamonds, carbon black and multiwalled nanotubes in electrical double layer capacitors. Carbon **45**, 2511–2518 (2007). doi:10.1016/j.carbon.2007.08.024
109. C. Portet, J. Chmiola, Y. Gogotsi, S. Park, K. Lian, Electrochemical characterizations of carbon nanomaterials by the cavity microelectrode technique. Electrochim. Acta **53**, 7675–7680 (2008). doi:10.1016/j.electacta.2008.05.019
110. Y.Q. Sun, Q. Wu, Y.X. Xu, H. Bai, C. Li, G.G. Shi, Highly conductive and flexible mesoporous graphitic films prepared by graphitizing the composites of graphene oxide and nanodiamond. J. Mater. Chem. **21**, 7154–7160 (2011). doi:10.1039/C0JM04434B
111. S. Park, K. Lian, Y. Gogotsi, Pseudocapacitive behavior of carbon nanoparticles modified by phosphomolybdic acid. J. Electrochem. Soc. **156**, A921–A926 (2009). doi:10.1149/1.3223964
112. J. Zang, Y. Wang, X. Zhao, G. Xin, S. Sun, X. Qu, S. Ren, Electrochemical synthesis of polyaniline on nanodiamond powder. Int. J. Electrochem. Sci. **7**, 1677–1687 (2012)
113. I. Kovalenko, D.G. Bucknall, G. Yushin, Detonation nanodiamond and onion-like-carbon-embedded polyaniline for supercapacitors. Adv. Func. Mater. **20**, 3979–3986 (2010). doi:10.1002/adfm.201000906
114. A. Kausar, R. Ashraf, M. Siddiq, Polymer/nanodiamond composites in Li-ion batteries: a review. Polymer-Plast Technol. **53**, 550–563 (2014). doi:10.1080/03602559.2013.854386

115. W. Gu, N. Peters, G. Yushin, Functionalized carbon onions, detonation nanodiamond and mesoporous carbon as cathodes in li-ion electrochemical energy storage devices. Carbon **53**, 292–301 (2013). doi:10.1016/j.carbon.2012.10.061
116. E. Tamburri, S. Orlanducci, V. Guglielmotti, G. Reina, M. Rossi, M.L. Terranova, Engineering detonation nanodiamond–polyaniline composites by electrochemical routes: structural features and functional characterizations. Polymer **52**, 5001–5008 (2011). doi:10.1016/j.polymer.2011.09.003
117. H. Gomez, M.K. Ram, F. Alvi, E. Stefanakos, A. Kumar, Novel synthesis, characterization, and corrosion inhibition properties of nanodiamond-polyaniline films. J. Phys. Chem. C **114**, 18797–18804 (2010). doi:10.1021/jp106379e
118. Z. Zhao, Y. Dai, Nanodiamond/carbon nitride hybrid nanoarchitecture as an efficient metal-free catalyst for oxidant- and steam-free dehydrogenation. J. Mater. Chem. A **2**, 13442–13451 (2014). doi:10.1039/C4TA02282C
119. A.E. Fischer, G.M. Swain, Preparation and characterization of boron-doped diamond powder: a possible dimensionally stable electrocatalyst support material. J. Electrochem. Soc. **152**, B369–B375 (2005). doi:10.1149/1.1984367
120. A. Ay, V.M. Swope, G.M. Swain, The physicochemical and electrochemical properties of 100 and 500 nm diameter diamond powders coated with boron-doped nanocrystalline diamond. J. Electrochem. Soc. **155**, B1013–B1022 (2005). doi:10.1149/1.2958308
121. J. Zang, Y. Wang, H. Huang, W. Tang, Electrochemical behavior of high-pressure synthetic boron doped diamond powder electrodes. Electrochim. Acta **52**, 4398–4402 (2007). doi:10.1016/j.electacta.2006.12.028
122. L. Cunci, C.R. Cabrera, Preparation and electrochemistry of boron-doped diamond nanoparticles on glassy carbon electrodes. Electrochem. Solid-State Lett. **14**, K17–K19 (2011). doi:10.1149/1.3532943
123. S. Heyer, W. Janssen, S. Turner, Y.-G. Lu, W.S. Yeap, J. Verbeeck, K. Haenen, A. Krueger, Toward deep blue nano hope diamonds: heavily boron-doped diamond nanoparticles. ACS Nano **8**, 5757–5764 (2014). doi:10.1021/nn500573x
124. A.A.V.M. Swope, G.M. Swain, The Physicochemical and electrochemical properties of 100 and 500 nm diameter diamond powders coated with boron-doped nanocrystalline diamond. J. Electrochem. Soc. **155**, B1013–B1022 (2005). doi:10.1149/1.2958308
125. G.R. Salazar-Banda, K.I.B. Eguiluz, L.A. Avaca, Boron-doped diamond powder as catalyst support for fuel cell applications. Electrochem. Comm. **9**, 59–64 (2007). doi:10.1016/j.elecom.2006.08.038
126. C.Y. Ko, J.H. Huang, S. Raina, W.P. Kang, A high performance non-enzymatic glucose sensor based on nickel hydroxide modified nitrogen-incorporated nanodiamonds. Analyst **138**, 3201–3208 (2013). doi:10.1039/C3AN36679K
127. N. Spătaru, X. Zhang, T. Spătaru, D.A. Tryk, A. Fujishima, Anodic Deposition of RuO x·nH2O at conductive diamond films and conductive diamond powder for electrochemical capacitors. J. Electrochem. Soc. **155**, D73–D77 (2008). doi:10.1149/1.2804379
128. S.K. Lee, M.J. Song, J.H. Kim, T.S. Kan, Y.K. Lim, J.P. Ahn, D.S. Lim, 3D-networked carbon nanotube/diamond core-shell nanowires for enhanced electrochemical performance. NPG Asia Mater. **6**, e115 (2014). doi:10.1038/am.2014.50
129. C. Dincer, E. Laubender, J. Hees, C.E. Nebel, G. Urban, J. Heinze, SECM detection of single boron doped diamond nanodes and nanoelectrode arrays using phase-operated shear force technique. Electrochem. Commun. **24**, 123–127 (2012). doi:10.1016/j.elecom.2012.08.005
130. C. Dincer, R. Ktaich, E. Lauberder, J.J. Hees, J. Kieninger, C.E. Nebel, J. Heinze, G.A. Urabn, Nanocrystalline boron-doped diamond nanoelectrode arrays for ultrasensitive dopamine detection. Electrochim. Acta. **185**, 101–106 (2015). doi:10.1016/j.electacta.2015.10.113
131. J. Hees, R. Hoffmann, A. Kriele, W. Smirnov, H. Obloh, K. Glorer, B. Raynor, R. Driad, N. Yang, O.A. Williams, C.E. Nebel, Nanocrystalline diamond nanoelectrode arrays and ensembles. ACS Nano **5**, 339–3346 (2011). doi:10.1021/nn2005409

132. J. Hees, R. Hoffmann, N. Yang, C.E. Nebel, Diamond nanoelectrode arrays for the detection of surface sensitive adsorption. Chem. Euro. J. **19**, 11287–11292 (2013). doi:10.1002/chem.201301763
133. F. Gao, C.E. Nebel, Diamond nanowire forest decorated with nickel hydroxide as a pseudocapacitive material for fast charging-discharging. Phys. Status. Solidi. A. **212**, 2533–2538 (2015). doi:10.1002/pssa.201532131
134. F. Gao, C.E. Nebel, Diamond-based supercapacitors: realization and properties. ACS Appl. Mater. Interfaces (2016). doi:10.1021/acsami.5b07027
135. F. Gao, R. Thomann, C.E. Nebel, Aligned Pt-diamond core-shell nanowires for electrochemical catalysis. Electrochem. Commun. **50**, 32–35 (2015). doi:10.1016/j.elecom.2014.11.006
136. Q. Wang, N. Plylahan, M.V. Shelke, R.R. Devarapalli, M. Li, P. Subramanian, T. Djenizian, R. Boukherroub, S. Szunerits, Nanodiamond particles/reduced graphene oxide composites as efficient supercapacitor electrodes. Carbon **68**, 175–184 (2014). doi:10.1016/j.carbon.2013.10.077
137. N. Yang, J.S. Foord, X. Jiang, Diamond electrochemistry at the nanoscale: A review. Carbon **99**, 90–110 (2016). doi:10.1016/j.carbon.2015.11.061
138. Y. Liu, S. Chen, X. Quan, H. Yu, Efficient electrochemical reduction of carbon dioxide to acetate on nitrogen-doped nanodiamond. J. Am. Chem. Soc. **137**, 11631–11636 (2015). doi:10.1021/jacs.5b02975
139. D. Aradilla, F. Gao, G. Lewes-Malandrakis, W. Muller-Sebert, D. Gaboriau, P. Gentile, B. Iliev, T. Schubert, S. Sadki, G. Bidan, C.E. Nebel. A step forward into hierarchically nanostructured materials for high performance micro-supercapacitors: Diamond-coated SiNW electrodes in protic ionic liquid electrolyte. Electrochem. Commun. **63**, 34–38 (2016). doi:10.1016/j.elecom.2015.12.008
140. T.T. Thanh, H. Ba, L. Truong-Phuoc, J.-M. Nhut, O. Ersen, D. Begin, I. Janowska, D.L. Nguyen, P. Granger, C. Pham-Huu, A few-layer graphene–graphene oxide composite containing nanodiamonds as metal-free catalysts. J. Mater. Chem. A. **2**, 11349–11357 (2014). doi:10.1039/C4TA01307G
141. H. Krysova, L. Kavan, Z.V. Zivcova, W.S. Yeap, P. Verstappen, W. Maes, K. Haenen, F. Gao, C.E. Nebel, Dye-sensitization of boron-doped diamond foam: champion photoelectrochemical performance of diamond electrodes under solar light illumination. RSC Adv. **5**, 81069–81077 (2015). doi:10.1039/C5RA12413A
142. D.W.M. Arrigan, Nanoelectrodes, nanoelectrode arrays and their applications. Analyst **129**, 1157–1165 (2004). doi:10.1039/B415395M
143. R.G. Compton, G.G. Wildgoose, N.V. Rees, I. Streeter, R. Baron, Design, fabrication, characterisation and application of nanoelectrode arrays. Chem. Phys. Lett. **459**, 1–17 (2008). doi:10.1016/j.cplett.2008.03.095
144. J. Guo, E. Lindner, Cyclic voltammograms at coplanar and shallow recessed microdisk electrode arrays: guidelines for design and experiment. Anal. Chem. **81**, 130–138 (2009). doi:10.1021/ac801592j
145. M. Fleischmann, S. Pons, J. Daschbach, The ac impedance of spherical, cylindrical, disk, and ring microelectrodes. J. Electroanal. Chem. **317**, 1–26 (1991). doi:10.1016/0022-0728(91)85001-6
146. M. Fleischmann, S. Pons, The behavior of microdisk and microring electrodes. Mass transport to the disk in the unsteady state: the ac response. J. Electroanal. Chem. **250**, 277–283 (1988). doi:10.1016/0022-0728(88)85169-6
147. N. Yang, S.R. Waldvogel, X. Jiang, Electrochemistry of carbon dioxide on carbon electrodes. ACS Appl. Mater. Interfaces (2016). doi:10.1021/acsami.5b09825
148. N. Yang, G.M. Swain, X. Jiang, Nanocarbon electrochemistry and electroanalysis: current status and future perspectives. Electroanalysis **28**, 27–34 (2016). doi:10.1002/elan.201500577